HHS Public Access

Author manuscript

Cell. Author manuscript; available in PMC 2018 November 02.

Published in final edited form as:

Cell. 2017 November 02; 171(4): 849–864.e25. doi:10.1016/j.cell.2017.10.005.

Plexin-B2 mediates physiologic and pathologic functions of angiogenin

Wenhao Yu[1,2,6], **Kevin A. Goncalves**[1,3,6], **Hiroko Kishikawa**[1,2], **Shuping Li**[1,2], **Guangjie Sun**[2], **Hailing Yang**[1,3], **Nil Vanli**[1,4], **Yunxia Wu**[2], **Yuxiang Jiang**[1], **Miaofen G. Hu**[1], **Roland H. Friedel**[5], and **Guo-fu Hu**[1,2,3,4,7,*]

[1]Molecular Oncology Research Institute, Tufts Medical Center, 800 Washington Street, Boston, MA 02111

[2]Department of Pathology, Harvard Medical School, 77 Avenue Louis Pasteur, Boston, MA 02115

[3]Graduate Program in Cellular and Molecular Physiology, Sackler School of Graduate Biomedical Sciences, Tufts University, 145 Harrison Avenue, Boston, MA 02111

[4]Graduate Program in Biochemistry, Sackler School of Graduate Biomedical Sciences, Tufts University, 145 Harrison Avenue, Boston, MA 02111

[5]Department of Neuroscience, Icahn School of Medicine at Mount Sinai, 1425 Madison Avenue, New York, NY 10029

SUMMARY

Angiogenin (ANG) is a secreted ribonuclease (RNase) with cell type- and context-specific roles in growth, survival, and regeneration. Although these functions require receptor-mediated endocytosis and appropriate subcellular localization, the identity of the cell surface receptor remains undefined. Here, we show that plexin-B2 (PLXNB2) is the functional receptor for ANG in endothelial, cancer, neuronal, and normal hematopoietic and leukemic stem and progenitor cells. Mechanistically, PLXNB2 mediates intracellular RNA processing that contribute to cell growth, survival, and regenerative capabilities of ANG. Antibodies generated against the ANG binding site on PLXNB2 restricts ANG activity *in vitro* and *in vivo*, resulting in inhibition of established xenograft tumors, ANG-induced neurogenesis and neuroprotection, levels of pro-self-renewal transcripts in hematopoietic and patient-derived leukemic stem/progenitor cells, and reduced progression of leukemia *in vivo*. PLXNB2 is therefore required for the physiological and pathological functions of ANG and has significant therapeutic potential in solid and hematopoietic cancers and neurodegenerative diseases.

[*]Correspondence: guo-fu.hu@tufts.edu.
[6]These authors contributed equally
[7]Lead Contact

AUTHOR CONTRIBUTIONS

G.H. conceived and supervised the project. W.Y., K.A.G., H.K., S.L., G.S., H.Y., N.V., Y.W., Y.J., M.G.H., R.H.F., and G.H. designed and performed the experiments and analyzed the data. W.Y., K.A.G., and G.H. wrote the manuscript.

In Brief

Plexin-B2 acts as a functional angiogenin receptor in a variety of physiological and pathological contexts, suggesting that the ANG-PLXNB2 axis could be harnessed for therapeutic applications.

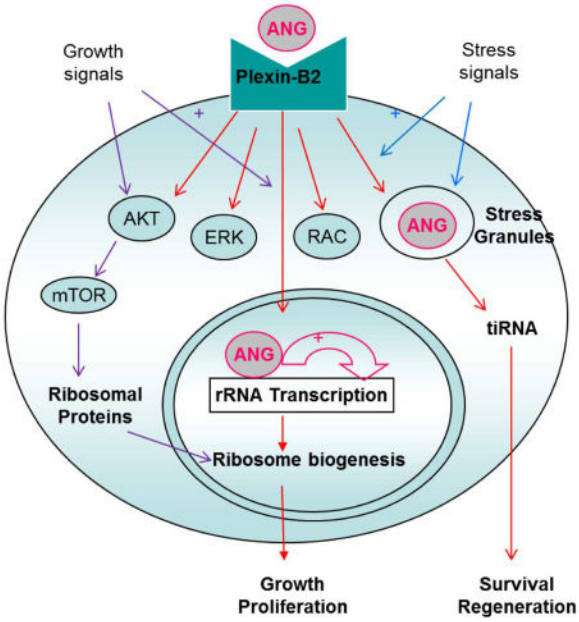

INTRODUCTION

Angiogenin (ANG) is a secreted ribonuclease (Marx, 1985) that has been shown to regulate fundamental cellular processes in both physiological and pathological cell types. ANG expression is altered in various human cancers and in neurodegenerative diseases. Loss-of-function mutations in the coding region of *ANG* have been found in amyotrophic lateral sclerosis (ALS) and Parkinson's disease (PD) patients (Greenway et al., 2006; van Es et al., 2011). ANG has a wide tissue distribution (Weiner et al., 1987) and its biological activities are diverse including regulation of cell growth and survival (Li and Hu, 2012), neurogenesis and neuroprotection (Subramanian and Feng, 2007), innate immune reactions (Hooper et al., 2003), and hematopoietic stem/progenitor cell (HSPC) growth and survival (Goncalves et al., 2016; Silberstein et al., 2016). ANG inhibitors reduce cancer growth and survival (Yoshioka et al., 2006), while supplemental therapy with ANG protein prolongs survival of ALS model mice (Kieran et al., 2008) and promotes hematopoietic regeneration following bone marrow (BM) failure in stem cell transplantation of clinically-relevant human cord blood cells (Goncalves et al., 2016).

ANG is known to be internalized via receptor-mediated endocytosis and undergo cell type- and context-specific differential subcellular localization. Under growth conditions and in differentiated cells, ANG is translocated to the nucleus and stimulates ribosomal RNA (rRNA) transcription, thereby promoting cell growth and proliferation. Under stress conditions or in primitive cells, ANG is translocated to stress granules (SGs) and mediates production of tRNA-derived stress-induced small RNA (tiRNA), which reprograms protein

synthesis by suppressing global protein translation to save anabolic energy while permitting IRES-mediated translation (Ivanov et al., 2011), a mechanism often used by anti-apoptotic genes. Thus, the cell surface receptor is essential for ANG to exert its biological activities, and is a promising target for ANG-related therapies (Di Scala and Hidalgo, 2016). However, the identity of this receptor remains unknown.

In this report, we demonstrate that plexin-B2 (PLXNB2) is both necessary and sufficient to mediate the biological activities of ANG in physiologically-, pathologically-, and therapeutically-relevant cell types, including endothelial, cancer, neuronal, and normal and malignant stem and progenitor cells. We show that PLXNB2 mediates cellular activities of ANG including nuclear translocation, SG localization, rRNA transcription, tiRNA production, AKT and ERK phosphorylation, Rac and Cdc42 activation, as well as cell growth, stem cell self-renewal, survival, and regenerative capabilities. Further, we establish that modulation of ANG-PLXNB2 activities is therapeutically relevant in a number of pathological conditions including solid and blood cancers, neurodegenerative diseases, and hematopoietic regeneration.

RESULTS

PLXNB2 is the functional cell surface receptor of ANG

ANG was originally identified as a tumor angiogenic factor (Fett et al., 1985). Endothelial cells were thus extensively used in previous attempts for identification of ANG receptors. However, this strategy has been unproductive as the receptor in endothelial cells is down-regulated when cell density increases (Hu et al., 1997). As ANG was also found to stimulate LNCaP proliferation in the absence of androgen (Li et al., 2013), we used LNCaP as the target cells and found that ^{125}I-ANG binds to LNCaP cells specifically (Figure 1A) with a K_d of 0.45 nM (Figure 1B). Affinity chromatography on ANG-Sepharose revealed a prominent band with apparent MW of ~175 kDa (Figure 1C). This band did not appear in the eluate from a non-affinity Sepharose column and its abundance was reduced when the sample was pre-incubated with free ANG, indicating that it is specific for ANG. Mass spectrometry analysis revealed that 15 peptides were matched to human PLXNB2 (Figure 1D). PLXNB2, originally identified from malignant brain tumors (Shinoura et al., 1995), is known to play an important role in neuronal development and glioma malignancy (Daviaud et al., 2016; Deng et al., 2007; Friedel et al., 2007; Le et al., 2015). PLXNB2 expression is widespread during development, but is more restricted in adult tissues, mainly in neural stem cells (Saha et al., 2012), functionally specialized endothelial cells and certain endocrine organs (Zielonka et al., 2010). RT-PCR showed that *PLXNB2* expression is density-dependent in human umbilical vein endothelial cells (HUVEC) but density-independent in LNCaP cells (Figure 1E), consistent with the observation that the activity of ANG in HUVEC is density-dependent (Hu et al., 1997) but is constitutive in cancer cells (Tsuji et al., 2005). Immunofluorescence (IF) confirmed that PLXNB2 is expressed on LNCaP cell surface (Figure 1F). Meta-analysis of publically available array experiments shows that *PLXNB2* level in neoplasm is significantly higher ($p<10^{-10}$) than in normal tissues and cells, and other diseases (Figure S1A). Over-production of PLXNB2 protein in various human cancers (Figure S1B-D) and in mouse tumors (Figure S1E-F) was confirmed by

immunohistochemistry (IHC), and correlates with significantly reduced median survival in patients with prostate cancer (Figure S1G), glioma (Figure S1H), and breast cancer (Figure S1I).

To obtain biochemical evidence that ANG indeed binds to PLXNB2, we expressed the Sema domains of PLXNB2, purified it to homogeneity (Figure S2A), and examined its interaction with ANG by surface plasmon resonance (SPR), and found that ANG binds to PLXNB2 with an apparent K_d of 0.74 nM (Figure 1G) and a steady-state K_d of 2.87 nM (Figure S2B). No appreciable binding was detected between ANG and the Sema domain of PLXNB1 (Figure S2C) or PLXNB3 (Figure S2D) by SPR. These results show that ANG binds to PLXNB2 specifically with a K_d in nM range. ELISA analyses also showed that ANG binds to both Sema domain and extracellular domain (ECD) of PLXNB2 but not to that of PLXNB3 (Figure 1H). Ribonuclease 4 (RNASE4), a homologous protein of ANG, did not bind to PLXNB2 or PLXNB3 (Figure 1I).

Co-immunoprecipitation (Co-IP) demonstrated association of ANG with PLXNB2 *in vivo* (Figure 1J). Knockdown of *PLXNB2* expression in LNCaP cells (Figure 1K) abolished specific binding of ANG to cell surface (Figure S2E), inhibited nuclear translocation of ANG (Figure 1L), and abolished ANG-induced cell proliferation (Figure 1M), AKT and ERK phosphorylation, and 47S rRNA transcription (Figure 1N). *PLXNB2* knockdown also inhibited ANG-mediated tiRNA production (Figure 1O) and abolished the protective activity of ANG against starvation-induced apoptosis (Figure 1P). It is notable that ~30% tiRNA remained in *PLXNB2* knockdown cells, probably due to the residual PLXNB2 expressed in these cells. *PLXNB2* knockdown in PC3 (Figure S3A) and DU145 (Figure S3B) cells also resulted in decreased nuclear translocation of ANG (Figures S3C-D) and reduced cell proliferation (Figures S3E-F). Further, we observed reduced proliferation in glioblastoma cells (Figure S3G-F), breast cancer cells (Figure S3I-J), and chronic myelogenous leukemia (CML) cells (Figure S3K) following *PLXNB2* knockdown. Together, these data demonstrate that PLXNB2 is necessary for the biological activities of both endogenous and exogenous ANG in multiple cancer cell lines.

Ectopic expression of human *PLXNB2* in COS-7 cells, which express a low level of endogenous monkey *PlxnB2* (Figure 2A), enabled nuclear translocation of ANG (Figure 2B) and AKT phosphorylation (Figure 2C) upon ANG stimulation in these originally ANG-unresponsive cells. We found that ANG bound to the surface of *PLXNB2* transfectants of COS-7 at 4 °C (Figure S4A) and underwent nuclear translocation at 37 °C (Figure S4B). Ectopic expression of *PLXNB1* and *PLXNB3* in COS-7 cells (Figure 2D) did not enable nuclear translocation of ANG (Figure 2E). Moreover, biotinylated ANG bound to COS-7 cells transfected with *PLXNB2* but not to those transfected with *PLXNB1* and *PLXNB3* (Figure 2F). Together, these results indicate that PLXNB2 is a specific and functional receptor for ANG and is both necessary and sufficient to mediate the biological functions of ANG.

To identify the ANG binding site on PLXNB2, serial deletion mutants were prepared and transfected into COS-7 cells, and the ability of these transfectants to mediate nuclear translocation of ANG was examined. Deletion of the Sema domain eliminated nuclear

translocation of ANG (Figure 2G), whereas deletion of PSI and/or IPT domains had no effect. Further serial deletions were examined and the putative ANG binding site was identified to be located between residues 334 and 449 (Figure S4C). Then, a series of peptides of 15 amino acids covering this region were synthesized and their binding capacity to ANG was examined by equilibrium dialysis (Figure 2H), differential spectrum (Figure 2I), and ELISA (Figure 2J). Among the peptides examined, only hplb2-15-06 showed appreciable binding to ANG in all three assays. Next, we attempted to determine which one of the three functional sites of ANG is responsible for PLXNB2 binding. ANG has a receptor binding site, a catalytic center, and a nuclear localization sequence. Mutations at the receptor binding site of ANG (R66A and N68D) abolished binding to this peptide but mutations at the catalytic center (H13A) had no effect (Figure 2J). These results indicate that the receptor binding site of ANG is where PLXNB2 binds. We next examined the inhibitory activity of hplb2-15-06 towards ANG, and found that it inhibited nuclear translocation of ANG as did the Sema domain (Figure 2K), and inhibited ANG-induced angiogenesis (Figure 2L). The peptide from the adjacent sequence (hplb2-15-05) did not bind ANG (Figures 2H-J) and did not inhibit ANG activity (Figures 2K-L). These results demonstrate that the ANG binding site on PLXNB2 is located within hplb2-15-06 at amino acid residues 424-441 with a sequence of GTSSEYDSILVEINKRVK (Figure S4D). It is notable that the sequence of this binding site is only present in PLXNB2, and not conserved in PLXNB1 and PLXNB3 (Figure S4E) (Janssen et al., 2010). Based on the crystal structure of PLXNB1, ANG-binding site on PLXNB2 consists of the end of sixth blade (β6d) and part of the loop that connects the seventh blade (Figure S4E).

Monoclonal antibody (mAb) against the ANG-binding site of PLXNB2 inhibits tumor growth

Since the ANG-binding site on PLXNB2 is located on a beta-sheet strand and a linker loop with low steric constraints, we reasoned that a synthetic peptide containing this sequence could serve as an antigen to generate monoclonal antibodies (mAb) that would bind to PLXNB2 and blocks ANG binding to the same site. Indeed, mAbs generated using hplb2-15-06 as the immunogen bind both the synthetic peptide (Figure S5A), the ECD domain (Figure S5B) and the Sema domain (Figure S5C) of PLXNB2. A commercial mAb of PLXNB2 did not bind to the small peptide but bind to the ECD and Sema domains. These mAbs inhibited ANG-induced LNCaP cell proliferation with an IC^{50} ranging from 4 to 16 μg/ml (Figure S5D). Among them, mAb17 has the lowest IC50 and was thus used in subsequent experiments. First, we confirmed binding between PLXNB2 and mAb17 biochemically by SPR and determined the binding affinity to be 8.3×10^{-14} M (Figure 3A). Second, we performed flow cytometry analysis of LNCaP cells and showed that mAb17 binds to the surface of live cells (Figure 3B). Functionally, we showed that at 30 μg/ml, mAb17 completely blocked nuclear translocation of ANG under growth conditions (Figure 3C) and SG localization under stress (Figure 3D), and abolished angiogenic activity of both ANG and VEGF (Figure 3E) as we have shown before that ANG-mediated rRNA transcription is required for VEGF to induce angiogenesis (Kishimoto et al., 2005). Proliferation of solid and hematopoietic cancer cells was also inhibited by mAb17, including prostate (Figures 3F, S5D-E), breast (Figures S5F-G), and myeloid and lymphoid leukemia cells (Figures S5H-J), and GBM (Figure S5K). mAb17 had no effect on proliferation following doxycycline-induced, shRNA-mediated knockdown of *PLXNB2* in U87 cells

(Figure S5K). Quantitative flow cytometry analysis showed that these mAb17-responsive cells express considerable amount of PLXNB2 (Table S1). Even though a correlation between PLXNB2 expression and responsiveness to mAb17 could not be established, we found that treatment with mAb17 resulted in downregulation of *PLXNB2* in MCF7 cells (Figure S5L), and led to upregulation of pro-apoptotic transcripts and downregulation of pro-survival transcripts in U87 cells (Figure S5M).

The anti-tumor activity of PLXNB2 mAb was demonstrated in xenograft animal models. It completely prevented the establishment of PC-3 xenograft tumors in athymic mice (Figure 3G) and inhibited the growth of established xenograft by 80% (Figure 3H). *In vivo* treatment with mAb17 led to a reduction of cancer cell proliferation (Figure 3I) and tumor angiogenesis (Figure 3J). Notably, tumor tissues from mAb17-treated animals showed significantly stronger mouse IgG staining than those from PBS-treated animals (Figure 3K), indicating successful targeting of administered mAb to tumor tissues. In the mAb17-treated tumor tissues, nuclear translocation of ANG was inhibited (Figure 3L), and rRNA transcription was reduced as indicated by a 50% decrease in the number of nucleolar organizer region (NOR) (Figure 3M), which are loops of rDNA that are actively transcribed to rRNA (Trere et al., 1989). mAb17 also inhibited growth of established U87 xenograft tumors (Figure S6A). These results demonstrate that treatment with mAb17 blocked nuclear translocation of ANG and led to inhibition of rRNA transcription, angiogenesis, tumor cell proliferation, and eventual tumor growth.

We previously established that neamine has a potent anti-tumor activity by blocking nuclear translocation of ANG through an unknown mechanism (Hirukawa et al., 2005). Using *PLXNB2* transfectants of COS-7 cells, we found that neamine inhibits binding of ANG to PLXNB2 dose dependently in co-IP experiments (Figure S6B), and diminished binding of biotinylated ANG to cell surface (Figure S6C). Consequently, we found that neamine treatment inhibited growth of established PC-3 xenograft in athymic mice (Figure S6D), accompanied by reduced tumor cell proliferation (S6E), and tumor angiogenesis (Figure S6F). These data suggest that the mechanism of action of neamine is through inhibition of binding of ANG to PLXNB2.

PLXNB2 mediates the neurogenesis and neuroprotective activities of ANG

ANG has been implicated in ALS and PD and is known to stimulate neurite outgrowth of P19 cells and protect stress-induced degeneration of P19 neurons (Subramanian and Feng, 2007). In order to know if PLXNB2 mediates the neurological functions of ANG, we first examined its expression in P19 cells and found that mouse PLXNB2 is expressed on the surface of P19 cells as shown by IF (Figure 4A). Next, we examined the functional consequence of PLXNB2 mAb and found that mAb17 inhibited p19 cell proliferation (Figure 4B), and diminished the protective activity of ANG against serum starvation-induced apoptosis of P19 cells (Figures 4C). Further, mAb17 was found to inhibit nuclear translocation of ANG under growth condition (Figure 4D) and SG accumulation of ANG under stress (Figure 4E) in P19 cells. ANG was also found to activate AKT and S6K, and Rac and Cdc42 in P19 cells, and this activation was inhibited by mAb17 (Figure 4F). ANG did not activate RhoA, which is known to be activated by semaphorin 4C (Sema4C), another

ligand of PLXNB2 (Perrot et al., 2002). Consistently, mAb17 did not affect RhoA (Figure 4F). mAb17 also inhibited basal level AKT phosphorylation and GTP-Rac activation (Figure 4F), likely through the inhibition of endogenous ANG activity. These data demonstrate that ANG and Sema4C trigger different signaling pathways upon binding to PLXNB2. mAb17 also inhibited ANG-stimulated neurosphere formation (Figure 4G) and neurite outgrowth (Figure 4H) of P19 cells and mouse embryonic cortical neurons (Figure 4I). Furthermore, it abolished the protective activity of ANG against hypothermic stress-induced neurofilament fragmentation of mouse embryonic cortical neurons (Figure 4J) and P19 cell-derived axons (Figure 4K). Taken together, these results indicate that PLXNB2 mediates the neurogenic and neuroprotective activities of ANG.

ANG restricts proliferation of HSPC through PLXNB2

We next examined whether PLXNB2 is the functional receptor for ANG in the hematopoietic system. First, we measured PLXNB2 expression in various cell types of the hematopoietic lineage and found that PLXNB2 levels are the highest in stem cells compared to whole BM or lineage-positive cells at mRNA (Figure S7A) and protein (Figure S7B) levels. We then assessed whether ANG acts through PLXNB2 in hematopoiesis using genetic and antibody strategies. We conditionally deleted *Plxnb2* in hematopoietic cells by crossing a *Plxnb2*-floxed mice (Friedel et al., 2007) with polyinosinic:polycytidylic acid (pIpC)-inducible *Mx1-cre* mice (Figure S7C). Efficient deletion of *Plxnb2* in BM following pIpC induction was confirmed by PCR (Figure S7D).

HSPC from Mx1-specific $Plxnb2^{-/-}$ mice cycle more actively, compared to those from WT mice that were similarly treated with pIpC (Figure 5A). Increased cycling of Mx1-specific $Plxnb2^{-/-}$ primitive cells was also observed in long-term hematopoietic stem cells (LT-HSC), short-term HSC (ST-HSC), and multi-potent progenitors (MPP) (Figure S7E). Consistently, Mx1-specific $Plxnb2^{-/-}$ mice showed increased LT-HSC number in BM, and elevated peripheral blood (PB) cell counts relative to WT mice (Table S2). Further, Mx1-specific $Plxnb2^{-/-}$ BM cells displayed greater exhaustion in serial re-plating assays in methylcellulose (Figure 5B), phenocopying what we observed in $Ang^{-/-}$ mice (Goncalves et al., 2016). Notably, treatment with recombinant ANG protein had no effect on $Plxnb2^{-/-}$ BM cells, but significantly enhanced colony formation of WT BM cells in later passages (Figure 5B), suggesting that ANG requires PLXNB2 to enhance colony formation.

To further profile the hematopoietic function of PLXNB2, we treated WT or Mx1-specific $Plxnb2^{-/-}$ mice with either serial 5-FU injections (Figure S7F) or 7.75 Gy γ-irradiation (Figure S7G) and observed premature death of all Mx1-specific $Plxnb2^{-/-}$ animals. These data suggest that stem/progenitor response in Mx1-specific $Plxnb2^{-/-}$ mice phenocopies that observed in $Ang^{-/-}$ mice. *Plxnb2* mRNA levels were elevated in central BM (Figure S7H) and sorted HSPC and MyePro (Figure S7I) 24 hours post-irradiation; however no changes in *Plxnb2* expression were observed in BM niche cells upon irradiation (Figure S7J), suggesting that PLXNB2 expressed in hematopoietic cells, but not in niche cells, responded to radiation exposure. To assess the *in vivo* function of PLXNB2, we competitively transplanted $Mx1\text{-}cre^{+};WT$ or $Mx1\text{-}cre^{+};Plxnb2^{fl/fl}$ WBM into WT hosts and induced with pIpC at week 4 post-transplant (Figure 5C), and observed a multi-lineage defect in long-

term reconstitution over 20 weeks post-transplant in mice transplanted with *Mx1-cre*$^{+}$*;Plxnb2*$^{fl/fl}$ donors (Figure 5D), indicating that *Plxnb2*-deficient HSPC have defective post-transplant reconstitution.

We previously observed that treatment of LT-HSCs with recombinant ANG protein restricted cell proliferation, led to elevated levels of various pro-self-renewal transcripts, and resulted in significant improvement of post-transplant reconstitution (Goncalves et al., 2016). To directly assess whether ANG acts through PLXNB2 in regulating LT-HSC function, we cultured WT or Mx1-specific *Plxnb2*$^{-/-}$ LT-HSCs in the presence of ANG protein. Culture of WT LT-HSCs with ANG resulted in restricted proliferation (Figure 5E) and enhanced expression of pro-self-renewal genes including *p21*, *p27*, *p57*, *GATA3*, *vWF*, and *Bmi1* (Figure 5F), while culture of *Plxnb2*-deficient LT-HSCs with ANG did not alter cell proliferation (Figure 5E) or self-renewal gene expression (Figure 5F), indicating that ANG needs PLXNB2 to exert these functions.

To further investigate whether PLXNB2 is the ANG receptor in HSPC, we injected WT and *Ang*$^{-/-}$ mice with mAb17 and assessed cell cycling. Injection of WT mice with mAb17 resulted in more active cycling of HSPC (Figure 5G) including LT-HSC, ST-HSC, and MPP (Figure S7K); however, injection of *Ang*$^{-/-}$ mice with mAb17 had no difference in cycling of HSPC (Figure 5G) and subtypes (Figure S7K). Consistently, mAb 17-induced active cycling of LT-HSC in WT mice was accompanied by increased LT-HSC number (Table S3). These data indicate that neutralization of PLXNB2 in WT mice phenocopies *Ang*$^{-/-}$ mice and show that PLXNB2 neutralization has no effect on *Ang*$^{-/-}$ HSPC number or cycling, suggesting that ANG and PLXNB2 act in the same pathway in regulating HSPC properties.

The *in vivo* effect of mAb17 on hematopoiesis can be recapitulated *in vitro* by culturing WT or *Ang*$^{-/-}$ cells in the presence of ANG protein, PLXNB2 mAb17, or both. Culture of WT LT-HSC with ANG or mAb17 led to a decreased or increased cell density (Figure 5H), and enhanced or suppressed expression of pro-self-renewal genes (Figure 5I), respectively; however, ANG treatment in the presence of mAb17 did not alter cell proliferation (Figure 5H) or pro-self-renewal gene expression (Figure 5I). With *Ang*$^{-/-}$ LT-HSCs, ANG was able to restrict cell proliferation (Figure 5H) and enhance pro-self-renewal gene expression (Figure 5I) but mAb17 had no effect. However, mAb17 effectively blocked the effect of exogenous ANG in these cells. Together, these data suggest that ANG acts through PLXNB2 to restrict proliferation and enhance pro-self-renewal signature of LT-HSC. In contrast, treatment of WT cells with Sema4C led to enhanced proliferation (Figure 5J), and increased levels of *cyclin D1*, but not of any pro-self-renewal genes (Figure 5K). Further, mAb17 did not inhibit any of the Sema4C-induced cell proliferation and cyclin D1 expression. These data suggest that the function of PLXNB2 is ligand-specific: whereas ANG restricts proliferation and enhances pro-self-renewal transcript level through PLXNB2, Sema4C enhances proliferation and cycling of LT-HSC.

To confirm that ANG enhances post-transplant reconstitution through PLXNB2, we transplanted LT-HSCs that were treated *ex vivo* for 7 days with ANG, mAb17, or both (Figure 5L). Treatment of WT LT-HSC with ANG and mAb17 resulted in enhanced and reduced post-transplant reconstitution, respectively (Figure 5M). However, treatment with

ANG and mAb together did not produce any changes. BM homing of CFSE-labeled CD45.1 Lin^- cells was not affected by mAb17 treatment (Figure S7L). Together, these data demonstrate that ANG acts through PLXNB2 in regulation of HSPC properties.

ANG restrict LymPro and stimulates MyePro proliferation through PLXNB2

To interrogate whether ANG acts through PLXNB2 in lineage-restricted progenitor cell types, we examined cell cycle status of lymphoid-restricted progenitors (LymPro) and MyePro in Mx1-specific *Plxnb2*$^{-/-}$ mice. We observed that common lymphoid progenitors (CLPs) and pre-pro B cells cycle more actively in Mx1-specific *Plxnb2*$^{-/-}$ BM (Figure S7M). Consistently, *in vivo* treatment with mAb17 enhanced cycling of CLP and pre-pro B in WT mice but not that in *Ang*$^{-/-}$ mice (Figure S7N). Consistently, no appreciable differences in LymPro number were observable following *Plxnb2* knockout (Table S2) or PLXNB2 neutralization (Table S3).

MyePro (Figure 6A) and the subtypes common myeloid progenitor (CMP) and granulocyte-macrophage progenitor (GMP) (Figure S7O) cycled less actively in Mx1-specific *Plxnb2*$^{-/-}$ BM, accompanied by a decrease in CMP and GMP numbers (Table S2), while, no difference in cycling (Figure S7O) and number (Table S2) was noticed for *Plxnb2*$^{-/-}$ megakaryocyte-erythroid progenitor (MEP). Consistently, *in vivo* treatment with mAb17 resulted in an increased G0 proportion of MyePro (Figure 6B), CMP and GMP (Figure S7P) in WT but not *Ang*$^{-/-}$ mice. Together, these data indicate that ANG acts through PLXNB2 in regulating hematopoietic progenitor subsets.

ANG acts through PLXNB2 to regulate protein synthesis and differential RNA biogenesis in hematopoietic cells

We have shown that the dichotomous effect of ANG in HPSC and MyePro is mediated by differential regulation of tiRNA and rRNA, which suppress and enhance protein synthesis, respectively, in these two types of cells (Goncalves et al., 2016). In order to demonstrate that PLXNB2 mediates this hematopoietic function of ANG, we examined the effect of ANG on protein synthesis in WT and *Plxnb2*$^{-/-}$ cells using O-propargyl-puromycin (OP-Puro) (Signer et al., 2014). Treatment of WT HSPC with ANG resulted in reduced levels of protein synthesis, while treatment of WT MyePro resulted in enhanced protein synthesis (Figure 6C). *Plxnb2*$^{-/-}$ HSPC showed elevated levels of protein synthesis on their own but did not respond to ANG treatment (Figure 6C). While *Plxnb2*$^{-/-}$ MyePro displayed reduced protein synthesis, these cells also did not respond to exogenous ANG. Moreover, these trends were observable in cells at G0/G1 (Figure 6D), indicating that the effect is cell type specific but is not related to cell cycle status.

ANG has been shown to regulate protein synthesis through cell type-specific RNA processing events: in MyePro, cell proliferation is enhanced by ANG through induction of rRNA, and in HSPC, cell proliferation is restricted by ANG through production of tiRNA (Goncalves et al., 2016). Consistent with this observation, we found that ANG did not alter rRNA synthesis in both WT and *Plxnb2*$^{-/-}$ HSPC, but significantly enhanced rRNA (both 47S and 28S) transcription in WT but not *Plxnb2*$^{-/-}$ MyePro (Figure 6E). These data suggest that the rRNA-stimulating activity of ANG in MyePro is dependent on PLXNB2. We also

assessed tiRNA levels and observed significantly reduced tiRNA levels in *Plxnb2*$^{-/-}$ HSPC (Figure 6F). In WT HSPC, ANG enhanced tiRNA level while mAb17 decreased it (Figure 6G). Significantly, treatment of WT HSPC with ANG in the presence of mAb17 failed to increase tiRNA levels. Together, these data suggest that ANG requires PLXNB2 to produce tiRNA in HSPC. The similarities in hematopoietic phenotypes and characteristics between *Ang*$^{-/-}$ and Mx1-specific *Plxnb2*$^{-/-}$ mice are listed in Table S4.

Targeting leukemic stem cells in CML therapy by ANG/PLXNB2 inhibitors

Given that the ANG-PLXNB2 axis regulates both cancer cells and primitive hematopoietic cells in a cell type-specific manner, we next assessed whether ANG-PLXNB2 would also regulate cancer stem cells. We first sorted CD34^{+}CD38^{-}, CD34^{+}CD38^{+}, and CD34^{-}CD38^{-} cells from CML patients both at chronic/stable phase (n=3) and blast phase (n=3) as well as from non-malignant control subjects (n=4) (Table S5) and measured PLXNB2 protein levels. We observed elevated levels of PLXNB2 in CD34^{+}CD38^{-} cells in BM aspirates from patients with blast phase CML, relative to those from chronic phase CML and non-malignant controls (Figure 7A). Treatment with ANG enhanced levels of pro-self-renewal transcripts in CD34^{+}CD38^{-} stem cells and CD34^{+}CD38^{+} primitive cells, but not in CD34^{-}CD38^{-} differentiated cells of both blast and chronic CML patients as well as non-malignant control subjects (Figure 7B). These data suggest that ANG regulates stemness of these primitive patient-derived cell types. Significantly, treatment with mAb17 led to a reduction in pro-self-renewal transcripts in stem and progenitor cells but not in differentiated cells (Figure 7B). It is significant that mAb17 had a greater magnitude effect in CD34^{+}CD38^{-} primary cells isolated from patients at blast phase than in those from chronic phase patients or from non-malignant controls, suggesting that anti-PLXNB2 therapy can de-regulate the self-renewal capabilities of cancer stem cells. Further, treatment of cells with ANG in the presence of mAb17 did not result in elevated pro-self-renewal transcript level (Figure 7B). Colony formation assays showed that the effect of ANG in regulating colony formation was abolished by mAb17 (Figure 7C). Significantly, mAb17 enhances CFU-GEMM formation only in blast phase cells (Figure 7C) further confirming its selective activities against primitive leukemia stem cells. Together, these data suggest that ANG may play an important role in growth of patient-derived human leukemic stem/progenitor cells, acts through PLXNB2, and may be therapeutically-targeted.

To further establish ANG/PLXNB2 inhibitors as candidate therapeutics, we examined the effect of mAb17 on hematological malignancies in immunocompetent mice utilizing a BCR-ABL mouse model of CML. GFP-BCR-ABL transduced BM cells were transplanted into sub-lethally irradiated WT mice, GFP+ cells from the first recipient mice were isolated and transplanted into secondary recipient mice, treated with mAb17 beginning immediately following engraftment for 2 weeks and analyzed for GFP positive cells in BM and PB (Figure 7D). In the PB, myeloid cell frequency was significantly diminished upon mAb17 treatment (Figure 7E), while in the BM, the number of primitive LKS cells (Figure 7F) or MyePro (Figure 7G) were significantly reduced with mAb17 treatment. Together, these data demonstrate that mAb17 has significant therapeutic potential in treatment of CML.

To assess the clinical utility of mAb17, we examined the potential toxicity and adverse side effect of prolonged treatment of mAb17 in immunocompetent mice, focusing on neurological and hematopoietic systems. Treatment with mAb17 twice a week at 30 mg/kg for two weeks (Figure S6G) had no effect on body weight and rotarod performance (Figure S6H), suggesting no significant toxicity or adverse effect on neuromuscular coordination. Treatment with mAb17 also did not result in abnormal hematopoiesis in the PB (Figure S6I-K) and BM (Figure S6L-Q) with only a modest decrease in HSPC and MyePro numbers (Figure S6L-N), consistent with the results obtained from a single injection of the antibody in WT mice (Table S3). These results indicate that long-term treatment of mAb17 does not result in overt neurological or hematopoietic defects.

DISCUSSION

In this report, we demonstrate that PLXNB2 is the functional cell surface receptor for ANG in a variety of cell types, including endothelial, solid and hematopoietic cancers, neuronal, normal HSPC and committed progenitors, and leukemic stem/progenitor cells. This finding is particularly important, given the highly diverse, cell type-specific functions of ANG in stem/progenitor cells versus mature cell populations. In all cell types examined to date, ANG has two main functions: regulation of cell growth and survival. Our study demonstrates that these two functions of ANG are both mediated by PLXNB2.

Previous reports have established that ANG promotes the growth of cancer cells through rRNA transcription, and also leads to activation of AKT/ERK. Here, we demonstrate that PLXNB2 mediates both processes, and inhibitors against PLXNB2 significantly reduce cell growth *in vitro*. Notably, mAb17 prevents the growth of established prostate tumors and GBM in athymic mice, and BCR-ABL-induced CML in immunocompetent mice, highlighting the therapeutic potential of anti-PLXNB2 therapies. Since ANG was identified as a tumor angiogenic factor and shown to be universally upregulated in various cancers, numerous efforts have been made to target it for cancer therapy. ANG inhibitors including its mAb (Olson et al., 1995) and small molecules (Kao et al., 2002) have all been shown to inhibit tumor growth in experimental animals. However, the receptor for ANG has remained unknown despite extensive efforts, and the lack of mechanistic comprehension prevented further development of ANG inhibitors in cancer therapy. Identification and characterization of PLXNB2 as the functional ANG receptor in cancer and endothelial cells not only provides much needed mechanistic understanding for further preclinical development but also offers a novel molecular target for intervention in cancer therapy. In this regard, we have shown that mAb17, which targets the ANG-binding site of PLXNB2, has robust anti-cancer activity in mice without significant toxicities.

In contrast to its upregulation in human cancers, ANG is downregulated and/or loss-of-function mutated in neurodegenerative diseases including ALS and PD. Supplementary therapy with recombinant ANG protein significantly improved motor muscular function of $SOD1^{G93A}$ mice and prolonged their lifespan. However, further development of ANG into clinical use for ALS therapy has also been hampered by unclear mechanisms of action and unknown identity of its receptors. Our data indicate that PLXNB2 mediates the neurogenesis and neuroprotection activity of ANG. Identification of PLXNB2 as the functional ANG

receptor in neurological system will facilitate development of ANG-based ALS therapeutics. It is notable that PLXNB2 is expressed in neural stem cells (Saha et al., 2012). It will be of great interest to examine if and how ANG-PLXNB2 regulates neural stem cell quiescence and self-renewal.

In this study, we also demonstrated a functional role of ANG in malignant stem cell-containing BM aspirates from CML patients, and we established a cell type-specific function of ANG-PLXNB2 in a malignant stem cell-containing population. CML is a disease of stem and progenitor cells, and current standard-of-care approaches, including BCR-ABL kinase inhibitors lack complete effectiveness in eliminating LSC (Druker et al., 2001). Therefore, the identification of novel treatments that are effective in eradicating LSC is essential, particularly in relapsed patients. Our current data suggest that mAb17 would be an attractive approach to diminish the self-renewal advantage of blast cells, which contribute to disease relapse. Significantly, mAb17 treatment resulted in a greater magnitude reduction of pro-self-renewal gene expression in blast crisis cells, compared to those in chronic phase and non-malignant cells. Therefore, this approach holds great promise, as the ANG-PLXNB2 axis regulates both growth and survival properties of stem cells. Whether mAb17 has such a preferential effect on cell growth and survival of blast crisis $CD34^{+}CD38^{-}$ primitive cells is the subject of future studies but initial experiments have shown that mAb17 is effective in inhibiting BCR-ABL-induced CML in immunocompetent mice.

As PLXNB2 is highly expressed in other tumor cell types, our current study has broad implications for all cancer subtypes, particularly those with known stem cell-containing populations or bone metastatic properties. Taken together, these results demonstrate that PLXNB2 is the functional cellular receptor for ANG mediating both growth and survival activities in a variety of cell types and that this unique mechanism is applicable to multiple tissue types and organ systems. PLXNB2 may thus serve as a molecular target for drug development to ultimately control ANG activities that go awry in a number of pathological conditions.

STAR METHODS

CONTACT FOR REAGENT AND RESOURCE SHARING

Further information and requests for resources and reagents should be directed to and will be fulfilled by the Lead Contact, Guo-fu Hu (guo-fu.hu@tufts.edu).

EXPERIMENTAL MODEL AND SUBJECT DETALS

Humans—Ficoll-separated BM mononuclear cells from bone marrow aspirates of patients with CML were obtained from Tufts Medical Center in compliance with institutional guidelines, as approved by the Institutional Review Board (IRB) of Tufts Medical Center. A total of 12 subjects were involved, including 4 no malignancy control (1 female, 3 male), 3 chronic phase CML patients (2 female, 1 male), and 3 blast phase CML patients (1 female, 2 male). Previous procedures were unclear with these patients.

Animals—B6.Cg-Tg(Mx1-cre)1Cgn/J mice (male), B6.SJL mice (male and female), C57B6 mice (male and female), and inbred nude NU/J mice (male) were obtained from the

Jackson Laboratory. Generation and characterization of *Ang*$^{-/-}$ mice were previously described (Goncalves et al., 2016). Mx1-specific *Plxnb2*$^{-/-}$ mice were generated by crossing B6.Cg-Tg(Mx1-cre)1Cgn/J (The Jackson Laboratory) mice with *Plxnb2*$^{fl/fl}$ mice (Friedel et al., 2007) to obtain *Cre*$^{+}$*;Plxnb2*$^{fl/fl}$ mice, which were then administered pIpC i.p. every other day for 6 days. For assessment of baseline cell number and cycling, mice were analyzed 10 days post-induction, as previously established (Frelin et al., 2013). For transplantation studies, mice were induced at week 4 post-transplant. In all studies, cre-positive *Plxnb2*$^{+/+}$ (control) and *Plxnb2*$^{fl/fl}$ mice were equivalently treated. B6.SJL were purchased from The Jackson Laboratory. For all studies, age-matched 7–10 week old mice were used. Nude mice were housed in sterile cages; other animals were housed in standard cages. All animals were housed in Association for Assessment and Accreditation of Laboratory Animal Care (AAALAC) accredited animal facility of Tufts Medical Center, and were visited daily by staff veterinarians. All animal experiments were approved by Institutional Animal Care and Use Committee (IACUC) of Tufts Medical Center.

Cells—$CD34^{+}CD38^{-}$ and $CD34^{+}CD38^{+}$ cells (mixed genders, pooled sources) were cultured in StemSpan SFEM (Stem Cell Technologies), supplemented with stem cell factor, Flt3 ligand, IL6, and thrombopoietin (100 ng/ml, R&D). $CD34^{-}CD38^{-}$ cells (mixed genders, pooled sources) were cultured in RPMI 1640 + 10% FBS. Human umbilical vein endothelial (HUVE) cells (mixed genders, pooled sources) were purchased from Cell Systems Corp. and were maintained in human endothelial-SFM (Life Technologies) supplemented with 5% FBS and 5 ng/ml bFGF at 37°C in 5% humidified CO_2. Human embryonic kidney cell line HEK293 (female), prostate cancer cell lines LNCaP (male), PC-3 (male), and DU-145 (male), breast cancer cell lines MDA-MB231 (female) and MCF-7 (female), immortalized T lymphocyte cell line Jurkat (male), immortalized myelogenous leukemia cell lines K562 (female) and KU812 (male), glioblastoma cell line U-87 MG (male), and monkey kidney cell line COS-7 (male) were purchased from ATCC. Glioblastoma cell line U251 (male) was purchased from Sigma-Aldrich, KU812 and LNCaP cells were cultured in RPMI 1640 + 10% FBS. The other cell lines were cultured in DMEM + 10% FBS. For experiments to examine the effect of ANG on LNCaP, the cells were cultured in phenol red-free RPMI 1640 + 10% charcoal/dextran-treated FBS. All cells were cultured at 37°C under humidified 5% CO^2 Cell viability was determined by trypan blue exclusion method.

METHOD DETAILS

Affinity chromatography—An ANG-Sepharose column was prepared by coupling 5 mg ANG protein to a 1 ml HiTrap NHSactivated Sepharose HP column (GE Healthcare Life Sciences). LNCaP cells were cultured in regular medium to subconfluent (~$1 \times 10^5/cm^2$), washed three times with PBS, and detached by scraping. A total of 2×10^9 cells were resuspended at a density of 2×10^7 per ml in lysis buffer (20 mM Hepes, pH7.1, containing 5 mM KCl, 1 mM $MgCl_2$, and 1 × protease inhibitor cocktail including 1 mM PMSF). The cell suspension was homogenized with a tight-fitting Dounce homogenizer (20 strokes) and centrifuged at 1,000 g for 5 min. The supernatant was collected and the precipitates were resuspended in the original volume of lysis buffer, homogenized again by 5 strokes in Dounce homogenizer, and centrifuged at 1,000 g for 5 min. The two supernatants were

combined and centrifuged at 100,000 g for 30 min. The precipitates were dissolved in 10 ml of 10 mM Tris-HCl, pH7.6, containing 1% Triton X-100, 5 mM EDTA, 150 mM NaCl, and 0.1% BSA. The extracted plasma membrane fraction was precleared by passing through an inactivated HiTrap Sepharose column. The flow-through fraction was divided into 2 fractions equally. The first half was applied to the above ANG-Sepharose column and eluted with 1 M NaCl in 10 mM Tris-HCl, pH7.6. The second half was mixed with 0.5 mg ANG, incubated at room temperature (RT) for 30 min, and then applied to the ANG-Sepharose column for affinity chromatography. This experiment was repeated 3 times.

Antibody production—Polyclonal antibodies against human ANG, RNASE4, and PLXNB2 were generated through custom antibody service in ProMab Biotechnologies, Inc. The antigens for ANG and RNASE4 were recombinant ANG and RNASE4 proteins, respectively. The antigen for PLXNB2 was a 19-amino acid synthetic peptide containing the ANG binding site of PLXNB2 (DGTSSEYDSILVEINKRVK). Polyclonal antibodies were purified by affinity chromatography on a Protein A-sepharose column. Monoclonal antibodies of PLXNB2 were generated at ProMab Biotechnologies, Inc. The antigen was a 15-amino acid peptide (TSSEYDSILVEINKR) from the ANG binding site of PLXNB2. Initial immunization was done in 5 BALB/c mice. Titers were measured using an ELISA method. Sp2/0 mouse myeloma cells were used for fusion. A panel of 10 hybridoma cells was generated. Five of them generated function antibodies, which were purified by Protein A/G affinity chromatography. The clone 9F6E12 (mAb17) was used for most of the experiments.

Apoptosis—Cells were detached by trypsinization, pelleted, and washed with 4 °C PBS. The cells were re-suspended in 25 μl of 4°C PBS and mixed with 2 μl of the ethidium bromide (EB)/acridine orange (AO) dye mixture (100 μg/ml each of AO and EB in PBS) at RT for 5 min. Stained cells were placed on a clean microscope slide and covered with cover slips. A total of 750 cells were counted from each group.

BCR-ABL mouse model of CML—BM wells were collected from male C57BL/6 male mice that have been treated with a single i.v. injection of 5-FU at 200 mg/kg for 4 days, transduced with BCR-ABL twice by spin infection with high-titer, helper-free replication-defective GFP-BCR-ABL1 retrovirus stock, and transplanted (4.2×10^5 cells per mouse) into first recipient mice (male, n=10) that have been irradiated twice at 450 cGy each. Disease progression was monitored by flow cytometry analyses of GFP+ Mac1+ and Gr1+ cells. Four weeks later, the GFP+ cells were sorted from the BM of the first recipient mice and transplanted into secondary recipient mice (male, 2.2×10^6 cells per mouse). GFP+ cells were detected in PB after 10 days and the animals were separated into 2 groups (n=5–6) and treated with PBS or mAb17 at 20 mg/kg, q3d, i.p., for 2 weeks, and analyzed by flow cytometry for the frequency of GFP positive Mac1+Gr1+ cells in PB and the number of GFP positive LKS and MyePro in BM.

Bone marrow cellularity—Dissected femurs were flushed with 5 ml PBS supplemented with 2% FBS. Resuspended cells were vortexed and white blood cell counts were obtained

by VetScan HM5 instrumentation (Abaxis Veterinary Diagnostics). Unpaired two-tailed Student's t-test was used for statistical analysis. *p<0.05, **p<0.01, ***p<0.001.

Bone marrow transplantation—Recipient mice were lethally-irradiated 16 hours prior to transplantation with split dose total body irradiation (12 Gy total: 2 doses at 3 hours apart). For analysis of Mx1-specific *Plxnb2*$^{-/-}$ mice by transplantation, 5 × 10^5 Mx1-cre$^+$;*Plxnb2*$^{+/+}$ or Mx1-cre$^+$;*Plxnb2*$^{-/-}$ whole BM (CD45.2) were co-injected with 5 × 10^5 WT B6.SJL whole BM (CD45.1) into WT B6.SJL (CD45.1) recipient mice. Cells were allowed to engraft 4 weeks, and peripheral blood was harvested to ensure equal engraftment among experimental groups. At week 4, recipient mice were induced with pIpC, as indicated under "pIpC Induction". For analysis of cells cultured in the presence ANG and/or mAb17, WT LT-HSCs were harvested, washed once in PBS/2% FBS, and counted. 400 WT LT-HSCs (CD45.2) were co-injected with 10^6 WT B6.SJL whole BM cells (CD45.1) into WT B6.SJL (CD45.1) recipient mice. Peripheral blood was taken at 4 week time intervals up until 16 or 20 weeks post-transplant, as indicated, for all transplantation assays.

Cell cycle analysis—Following staining with cell surface markers, 1 × 10^7 red cell-depleted BMMNCs were fixed and permeabilized using Cytofix/Cytoperm Fixation/ Permeabilization Kit (BD) per manufacturer's instructions. Cells were stained with Ki67 FITC (BD, 1:10 in BD Perm/Wash buffer), washed, and then stained with DAPI (2 μg/ml) for 10 minutes, directly prior to analysis. 2 × 10^6 events per sample were acquired on a FACSAria flow cytometer. Unpaired two-tailed Student's t-test was used for statistical analysis. *p<0.05, **p<0.01, ***p<0.001.

Cell proliferation—Cells were seeded in 35-mm dish at a density of 1 – 4 × 10^4 cells per dish and treated with ANG or antibodies at the concentration indicated. At each time point, cells were trypsinized and cell number determined by coulter counter or hematocytometer. Medium was replenished every 72 h. In the experiments to determine the effect of mAb17 on cancer cell proliferation, MTT (Biosynth) assay was used in 96-well plate with a seeding density of 2–5 × 10^3 cells per well. In the experiment to determine the IC50 of the panel of mAbs on LNCaP cells, MTT assay was used with a seeding density of 2 × 10^4 per well and the incubation was terminated at 120 h. MTT (10 μl, 5 mg/ml) was added to the wells and incubated for 2.5 h. After aspiration, 100 μl of DMSO was added to each well and incubated for 5 min at 37°C to solubilize the bio-reduced colored MTT-formazan and to lyse the cells. The optical density was read at 570 nm in a microplate reader. MTT assays were performed in quadruplicates each time and repeated three times. Unpaired two-tailed Student's t-test was used for statistical analysis. *p<0.05, **p<0.01, ***p<0.001.

Cell surface markers for stem and progenitor subtypes—Hematopoietic stem and progenitor cell types were identified based on the following phenotypic cell surface markers: LKS (Lin$^-$c-Kit$^+$Sca1$^+$), MyePro (Lin$^-$c-Kit$^+$Sca1$^-$), LT-HSC (Flk2$^-$CD34$^-$ LKS), ST-HSC (Flk2$^-$CD34$^+$ LKS), MPP (Flk2$^+$CD34$^+$ LKS), CLP (Lin$^-$c-Kit^{med}Sca1^{med}IL7R$^+$ Flk2$^+$ B220$^-$), pre-pro B (Lin$^-$c-Kit^{med}Sca1^{med}IL7R$^+$ Flk2$^+$ B220$^+$), CMP (Lin$^-$c-Kit$^+$Sca1$^-$CD34$^+$CD16/32$^-$), GMP (Lin$^-$c-Kit$^+$Sca1$^-$CD34$^+$CD16/32$^+$), and MEP (Lin$^-$c-Kit$^+$Sca1$^-$CD34$^-$CD16/32$^-$).

Chimerism studies—Red cell-depleted peripheral blood cells were stained for 30 minutes on ice with antibodies against CD45.1 APC (eBioscience), CD45.2 Pacific Blue (Biolegend), CD11b PE-Cy7, Gr1 PE, CD45R/B220 FITC, and CD3ε APC-Cy7. Cells were analyzed using a LSRII flow cytometer.

Co-immunoprecipitation—Flag tagged ANG (ANG-Flag) was prepared by engineering a flag tag to the C-terminus of ANG and was expressed in the pET11 expression vector in E. coli as for wide type ANG. ANG-Flag (1 μg/ml) was added to the plasma membrane fraction of LNCaP cells and incubated at 4°C for 30 min. The mixture was then divided into 3 equal fractions, and incubated with 10 μg/ml of ANG mAb 26-2F, Flag mAb M2 (Sigma), and control non-immune mAb CCL130, respectively, at 4°C for 2 h. Protein A/G-Sepharose (20 μl) was added and the tubes were rotated at 4°C overnight. The precipitates were analyzed for PLXNB2 by immunoblotting with PLXNB2 pAb (R&D Systems). In another experiment, the mixture was divided into two fractions and immunoprecipitated by PLXNB2 mAb (R&D Systems) and control mAb CCL130, and analyzed for ANG by immunoblotting with ANG polyclonal antibody R113. Co-immunoprecipitation experiments were repeated once.

Complete blood counts—Peripheral blood was obtained by retro-orbital bleeding using heparinized micro-hematocrit capillary tubes (Fisherbrand), and collected in EDTA-coated Microtainer tubes (BD). Complete blood counts were assessed by VetScan HM5 instrumentation. Unpaired two-tailed Student's t-test was used for statistical analysis. *$p<0.05$, **$p<0.01$, ***$p<0.001$.

Differential UV spectrometry—ANG (13.8 μM) and the testing peptide (30 μM) were dissolved in 15 mM Hepes, pH 7.0, containing 150 mM NaCl and put in the two compartments of a split cuvette. UV spectrum from 180 nm to 340 nm was recorded on a Beckman Coulter DU730 spectrophotometer. Then, the partition between the two compartments was removed and the two solutions were mixed, and the spectrum was again recorded. The difference in absorbance at 280 nm prior and post mixing was used as an indication for interactions between ANG and peptides.

ELISA—For determining the binding between ANG and peptides, the 96-well plates were coated with peptides at 2.5 μg/ml in PBS overnight at 4°C. The wells were blocked with 10 mg/ml BSA in PBS. ANG, or the variants (R66A, N68D, and H13A) were diluted to a final concentration of 10 ng/ml in PBS containing 5 mg/ml BSA and 0.02% Tween 20, added to the well (100 μl) and incubated at 4°C overnight. Bound ANG was detected by ANG monoclonal antibody 26-2F at 0.25 μg/ml and alkaline phosphatase conjugate of rabbit anti-mouse IgG (1.25 μg/ml). Absorbance at 405-410 nm was recorded on an ELISA plate reader after color development in 0.5 mg/ml p-nitrophenyl phosphate (Sigma) in 0.2 M diethanolamine buffer, pH9.8. For determining the binding between ANG or RNASE4 and PLXNB2, PLXNB3, or the Sema domain for PLXNB2, ELISA plates were coated with 0.1 μg/ml PLXNB2, PLXNB3, or the Sema domain of PLXNB2 in 10 mM sodium bicarbonate buffer, pH 8.3, at RT overnight. The wells were blocked with 3% BSA in PBS containing 0.05% Tween-20 for 1 h at RT, and incubated with ANG or RNASE 4 at concentrations

ranging from 25 to 200 ng/ml. Bound ANG and RNASE4 were detected with polyclonal antibodies against ANG and RNASE4, respectively, followed with alkaline phosphatase conjugate of goat anti-rabbit IgG as described above. ELISA experiments were performed in duplicates and repeated twice.

Equilibrium dialysis—An equilibrium dialysis chamber of 50 μl capacity was used. The two compartments of the chamber were divided with a dialysis membrane with a molecular weight cutoff of 6–8 KDa. ANG (89.9 μM) and the testing peptides (300 μM) were dissolved in 15 mM Hepes, pH 7.0, containing 150 mM NaCl and put in the two compartments, respectively. The initial concentration of ANG and peptides were recorded by absorbance at 280 nm. The chamber was tightly closed and put at RT for 24 h with occasional shaking with hands. At the end of incubation, the absorbance of solutions in both chambers was measured and the increase in ANG chamber was used to calculate the binding constants.

Expression and purification of Sema domains of PLXNB1, PLXNB2, and PLXNB3—Sema4C fusion protein was expressed and purified as His-tagged (C-terminus) fusion protein from HEK293 cells from HEK293 cells using pCI-neo as the expression vector. The Sema domains of human PLXNB1, PLXNB2, PLXNB3 were expressed as fusion proteins with mouse IgG1 Fc (C-terminus) in FreeStyle 293F cells. The nucleotide sequences of human PLXNB1, PLXNB2, PLXNB3 were from Genebank with number AB007867, AB002313, and AB033032 respectively. The SEMA region of human PLXNB1, PLXNB2, PLXNB3 are according to the Uniprot record with access number O43157 (PLXNB1, SEMA domain 20-479), O15031 (PLXNB2, SEMA domain 20-466), and Q9ULL4 (PXLNB3, SEMA domain 45-471). The mammalian expression vector pCMV3-untagged (from Sino Biological) was used and the cloning sites are *Hpa*I (5') and *EcoR*V (3'). The signal peptide human PLXNB1, PLXNB2, PLXNB3 were kept for effective secretion of expressed recombinant protiens. The sequences of primers are listed as following (the UPPERCASE letters are link region, and lowercase letters are target region): PLXNB1-F: 5'-GCTTGGTACCGCTAGCGGATCCGTT atgcctgctctgggcccagct-3' PLXNB1-R: 5'-TGTCGCGGGGCACAGAGCCTCCACCCCC cacaggaaccttcagaagtgtgctc-3' PLXNB2-F: 5'-GCTTGGTACCGCTAGCGGATCCGTT atggcactgcagctctgggc-3' PLXNB2-R: 5'-TGTCGCGGGGCACAGAGCCTCCACCCCC caccggcagccggaacaccttg-3' PLXNB3-F: 5'-GCTTGGTACCGCTAGCGGATCCGTT atgtgccacgccgcccaggag-3' PLXNB3-R: 5'-TGTCGCGGGGCACAGAGCCTCCACCCCC cacaggtatccggtccacctgg-3' linker-mIgG1-F: 5'-GGGGGTGGAGGCTCT gtgccccgcgacagcggctgca-3' mIgG1-R: 5'-CTCGAGTTTAAGCGCTATCGATGAT tcacttgccggggctgtggctcag-3'

PCR were performed with Platinum™ SuperFi™ PCR Master Mix (Thermo Fisher Scientific). The templates of PLXNB1, PLXNB2, and PLXNB3 gene were the expression vector pCI-neo carrying the PLXNBs whole genes as described above. Mouse IgG1 Fc gene were amplified from the cDNA of a mouse hybridoma secreted an antibody with IgG1 isotype (mAb17). PCR products were purified with the Select-A-Size DNA Clean & Concentrator kit (Zymo Research). After digestion of pCMV3 plasmid with *Hpa*I andd *EcoR*V-HF®, a band of ~6.1 kb was purified from agarose-TAE gel, transformed into

competent DH5α competent bacteria, plated on LB-agar plates with ampicillin selection reagent. All pCMV3 expression constructs were verified by DNA Sanger sequencing.

To express PLXNB (SEMA)-mIgG1 Fc fusion proteins, pCMV3 expression plasmids were purified and transfected into FreeStyle™ 293-F Cells (Thermo Fisher Scientific) at a cell density of 0.75×10^6 viable cells/ml and plasmid concentration of 1 μg/mL with 3 μg/mL PEI 25000 (Polysciences) plasmids. Transfected cells were cultured under 8% CO^2. On day 3 and day 5 post transfection, cells were supplied with CHO CD Efficient Feed™ B Liquid Nutrient Supplement (Thermo Fisher Scientific) at 5% of the volume of culture medium, and continued to culture for 2 more days. Culture medium were collected on day 7 post transfection by centrifugation at 1000 × g and filtration through 0.22 μm nylon membrane. The fusion proteins were purified with protein A agarose following the regular antibody purification procedure. The fusion proteins were further purified with HPLC on a size exclusion column Protein-Pak 300.

Flow cytometry analysis of cell surface PLXNB2 in LNCaP cells with mAb17— LNCaP cells, or PLXNB2 knockdown LNCaP cells (described below) were cultured in RPMI 1640 + 10% FBS to subconfluent, washed with 37 °C PBS twice, detached with 37 °C Versene (1.5 ml Versene to a 10 cm dish). When the cells started to round up, 3 ml complete medium was added to the dish, and the cells were collected, centrifuged at 800 × g, kept on ice, washed with ice-cold PBS twice, and resuspended in cold PBS + 2% FBS at a density of 1×10^6 cells per ml. For each staining, 150 μl cell suspension was used. mAb17 and IgG1k isotype control antibody was added at the final concentration of 5 μg/ml, and incubated on ice for 2 hours. Cells were pelleted, wash cells with cold PBS + 2% FBS, and incubated with PF conjugate of secondary antibody at 1:125dilution (eBioscience) on ice for 1 hour in dark. Cells were washed twice with PBS + 2% FBS, re-suspended in 400 μl PBS + 2% FBS, and analyzed on Cyan flow cytometer. Flow cytometry experiments were performed in duplicates and repeated twice.

Flow cytometry analysis of mouse PLXNB2—For determining mouse PLXNB2 levels by flow cytometry, cells were stained for 90 minutes on ice with antibodies against cKit BV711, Sca BV421 (Biolegend), Flk2 PE, CD34 FITC (eBioscience, 1:100), PLXNB2 APC (R&D, 1:5) and a biotynlated lineage cocktail, followed by staining with streptavidin Pacific Orange for 15 minutes on ice. Cells were analyzed using a LSRII flow cytometer. PLXNB2 protein levels were determined by quantification of geometric mean by flow cytometric analyses. For determining human PLXNB2 levels, cells were stained with 1 μg/ml PLXNB2 mAb 5P6, human CD34 APC (Biolegend), and human 38 PE (Biolegend) on ice for 45 minutes. Cells were then stained with FITC-labelled rabbit anti-mouse IgG (Molecular Probes, 1:400) on ice for 30 minutes. Cells were analyzed on a MoFlow Astrios flow cytometer.

Flow cytometry and cell sorting of hematopoietic cells—Tibias and femurs were dissected, crushed in PBS/2% FBS, and strained through 0.45 μm mesh to generate whole bone marrow mononuclear cells (BMMNC). ACK Lysis Buffer (Lonza) was used to deplete red blood cells by incubating cells on ice for 5 minutes with 2 ml lysis buffer, with periodic

vortexing. After washing, cells were stained in 200 μl PBS/2% FBS. Unless otherwise indicated, red celldepleted BMMNCs were stained with primary antibodies at 1:200 dilution.

5-Fluorouacil (5-FU) and irradiation treatment—5-FU was injected intraperitoneally at 150 mg/kg every 7 days. For one-time irradiation at 7.75 Gy, mice were irradiated with rotation (JL Shepherd irradiator) in a pie cage (Braintree Scientific). In order to ensure equal irradiation among groups, mice from different experimental groups were simultaneously irradiated in the same pie cage. For all studies, survival was assessed until 100% animal mortality was achieved. Unpaired two-tailed Student's t-test was used for statistical analysis. *p<0.05, **p<0.01, ***p<0.001

Genotyping—Genotyping was performed with standard PCR conditions on an iCycler PCR machine (Biorad). All PCR reactions were performed with Hot Start Green PCR Master Mix (Thermo Scientific). Primers for *Plxnb2*-floxed mice: PB2-EUC-F: 5'-TACTAGGATCAGAGGTCATCG-3'; PB2-EUC-R1: 5'-GCTTTGGTGTCAACTCCCAAG-3'; PB2-EUC-R2: 5'-CACAACGGGTTCTTCTGTTAGTCC-3'. Primers for $Ang^{-/-}$ mice: *Ang* primers, Forward, 5'-AGCGAATGGAAGCCCTTACA-3'; reverse, 5'-CTCATCGAAGTGGACAGGCA-3'. LoxP site primers (F12/B6): Forward, 5'-AGGGTGGAACTTCAGGATTCAAG-3'; reverse, 5'-GAAGTTATCCGCGGGAAGTTC-3'.

Homing assay—2×10^6 CD45.2 Lin^- cells were treated with 50 μg/ml mAb17, labeled with CFSE (Molecular Probes) per manufacturer's instructions, and transplanted into lethally-irradiated WT B6.SJL (CD45.1) recipient mice. 16 hours post-transplant, cells were harvested and stained with antibodies against cell-surface markers, as described above. Samples were analyzed on a FACSAria flow cytometer to determine percent CFSEpositive LKS cells and MyePro. Unpaired two-tailed Student's t-test was used for statistical analysis. *p<0.05, **p<0.01, ***p<0.001.

Immunoblotting—Cells were rinsed three times with PBS and lysed in RIPA lysis buffer (20 mM sodium phosphate, 150 mM NaCl, 5 mM sodium pyrophosphate, 5 mM EDTA, 1% Triton X-100, 0.5% sodium deoxycholate, 1 mM sodium orthovanadate, 0.1% SDS, pH 7.4) supplemented with 1 tablet/10 ml of complete mini-EDTA protease inhibitor cocktail (Roche). Cells were harvested with the aid of a rubber policeman, clarified by centrifugation at 15,000 g for 15 minutes at 4°C, and prepared for immunoblotting analysis. Total proteins (30–50 μg from clarified cell lysates) were separated via SDS-PAGE and electrotransferred onto nitrocellulose membranes (Santa Cruz Biotechnology). The membranes were blocked with Tris-buffered saline with Tween (0.5%) plus 5% dried nonfat milk for 30 minutes-1 hour at RT and probed with the desired primary antibody diluted in blocking buffer overnight at 4°C. β-actin or β-tubulin was used as loading control. Primary antibodies of ERK, p-ERK, AKT, p-AKT, and p-S6K (Cell Signaling) and of PLXNB2 (R & D Systems) were used per manufacturer's instructions. Incubation with the second antibody was carried out at RT for 1 h. β-actin and tubulin antibodies were from Santa Cruz Biotechnology and were used at a dilution of 1:600 and 1:200, respectively. For detecting Rho, Rac, and CDC42 activation, assay kits from Millipore were used per manufacturer's instructions. Proteins

were visualized with electrochemiluminescence detection reagents (Millipore) followed by autoradiography. Autoradiographs were quantified as described previously with ImageJ (NIH). The film was scanned using an HP Scanjet scanner.

Immunofluorescence and immunohistochemistry—For IF, cells were cultured on coverslips, fixed with −20°C methanol, washed 3 times with PBS, and blocked with 30 mg/ml BSA in PBS for 10 min at 37°C. Incubation with primary antibodies was done at 37°C for 1 h. The concentrations of mAbs used were 50 and 30 μg/ml for 26-2F and mAb17, respectively. The second antibodies (Alexa 488- or Alexa 555-labled goat F(ab')2 anti-mouse or -rabbit IgG, Molecular Probes) was used at 1:100 dilution. Nuclei were stained by 4',6-diamidino-2-phenylindole (DAPI, Molecular Probes). Images were taken under a Nikon Eclipse T*i* microscope. For IHC, tissue micro array and tissue sections were stained following standard laboratory practice. During antigen retrieval, slides were immersed in sodium citrate buffer (10mM Sodium Citrate, 0.05% Tween 20, pH 6.0) and with pressure cooker for 10 min (Cuisinart). Sections were blocked in 5% non-fat dry milk in PBS for 30 min and incubated with antibodies against PLEXNB2 (10 μg/ml, R&D Systems clone H-90 or in house mAb17), and human ANG (30 μg/ml, 26-2F) in 1% BSA in PBS at 4°C for 16 h. The slides were washed with PBS, and incubated with HRP-labeled secondary antibody (1:1000) and visualized with the DakoCytomation EnVision System (Dako).

***In vitro* and *In vivo* treatment with ANG, Sema4C and mAb17 in hematopoietic studies—**For *in vitro* analysis, cells were treated with 0.3 μg/ml ANG, 0.3 μg/ml Sema4C, 50 μg/ml mAb17, or the combinations as indicated. For *in vivo* analysis, mAb17 was injected intraperitoneally at 100 mg/mouse for three days.

***In vitro* angiogenesis assay—**Each well of the 48-well plate was coated with 50 μl growth factor-reduced Matrigel. HUVEC (1.5×10^4 per well) were seeded on the Matrigel and cultured in the presence or absence or testing materials for 4–5 h. ANG was used at 1 μg/ml, peptides were used at 25 μM, VEGF was used at 10 ng/ml, mAb17 was used at 30 μg/ml. Cells were fixed in 3.7% paraformaldehyde and photographed. The images were analyzed by ImageJ software to calculate the length or area of capillary-like structures as well as the numbers of circled tubular structure. Experiments were performed in triplicate and were repeated at least three times.

Leukemic stem/progenitor cell sorting—Patient samples were stained with human CD34 APC and human CD38 PE, and sorted on a MoFlow Astrios sorter. DAPI or 7-aminoactinomycin d (7-AAD, BD) were used as viability dyes for all analyses and sorts, per manufacturer's instructions. For bone marrow stem and progenitor analysis and lineage analysis, at least 2×10^6 and 3×10^4 events per sample were acquired, respectively. FlowJo X (Tree Star) was used to analyze data.

Lineage-positive Staining—Cells were stained for 30 minutes on ice with antibodies against CD11b PE-Cy7 (Biolegend), Gr1 PE (eBioscience, 1:400), CD45R/B220 FITC (BD), CD3ε APC-Cy7 (Biolegend), and Ter119 APC (eBioscience) and analyzed using a LSRII flow cytometer (BD).

LKS and MyePro sorting—Cells were stained for 30 minutes on ice with antibodies against cKit APC (eBioscience), Sca1 PE (eBioscience), and a FITC lineage cocktail. Cells were sorted using a MoFlow Astrios (Beckman Coulter) sorter.

LT-HSC sorting—Cells were stained for 90 minutes on ice with antibodies against cKit APC-eF780 (eBioscience), Sca1 PECy5, Flk2 PE, CD34 e660, and a biotinylated lineage cocktail, followed by staining with streptavidin PECy7 (Biolegend) for 15 minutes on ice. Cells were sorted using a FACSAria sorter.

Methylcellulose colony assays—For serial re-plating assay, colonies were scored by visualization on Day 7 post-inoculation of 2×10^4 whole BMMNCs in MethoCult M3434 methylcellulose. After scoring, colonies were harvested and 2×10^4 whole BMMNCs were plated in fresh methylcellulose, per manufacturer's instructions. Colonies were again scored on Day 7 post-inoculation. For experiments in which cells were treated with ANG (0.3 μg/ml), fresh ANG protein was added to cultures upon re-plating.

For human progenitor quantification, 2×10^4 human patient derived whole BM were plated in MethoCult H4034 methylcellulose in the presence or absence of 0.3 μg/ml human ANG. Colonies were scored by visualization, per manufacturer's recommendations. Unpaired two-tailed Student's t-test was used for statistical analysis. *p<0.05, **p<0.01, ***p<0.001

Mass spectrometry analysis—The eluates were separated in SDS-PAGE and visualized by silver staining. The bands of interest were excised from the gel, homogenized, and digested with proteomics grade trypsin (200 ng) in 50 mM NH_3HCO_3 in 10% acetonitrile overnight. The peptides were extracted by 50% acetonitrile and 5% acetic acid, dried by vacuum centrifugation, and submitted to the Mass Spectrometry Facility of Beth Israel Deaconess Medical Center for molecular mass analysis of the tryptic peptides. The identity of the proteins was determined by correlative searching of the Swiss-Prot protein database (swissprot_rev05/23/08) using Mascot (www.matrixscience.com).

Mouse LT-HSC culture—LT-HSCs were cultured at 37°C/5% CO^2 in S-clone SF-O3 (Sanko Junyaku) with the following supplements: 0.5% bovine serum albumin (Gibco Life Technologies), 50 ng/ml thrombopoietin (Peprotech), 50 ng/ml stem cell factor (Peprotech), 50 μM 2-mercaptoethanol (Gibco Life Technologies), and 1X Penicillin/Streptomycin (Corning). As indicated, cells were cultured in the presence or absence or ANG protein (0.3 μg/ml), Sema4C protein (0.3 μg/ml), IgG1-κ CCL130 isotype control (50 μg/ml), or mAb17 (50 μg/ml). At Day 7, cells were counted by hemocytometer for proliferation studies, harvested directly for qRT-PCR analyses (as described under "Quantitative RT-PCR Analyses of Hematopoietic Cells"), or washed once in PBS/2% FBS, counted, and transplanted into lethally-irradiated recipient animals.

Neurosphere formation and neurite outgrowth—P19 mouse embryonal carcinoma cells were normally maintained in DMEM + 10% FBS. For neurosphere formation and neurite outgrowth, P19 cell were seeded on PA6 monolayer and cultured in α-MEM plus 0.1% nonessential amino acids, 0.1% knockout serum replacement, 0.5 μM retinoic acid, and 200 ng/ml testing proteins for 24 h. Embryonal bodies from the entire well of 6-well

plates were counted under phase light microscope at 10X magnification. For neurite outgrowth, cells were cultured for 9 days and subjected to 40 min incubation at 16 °C, fixed in 4% paraformaldehyde for 15 min at RT followed with methanol for 5 min at −20 °C, blocked with 0.1% gelatin, 0.5% BSA and 0.1% Tween 20 in TBS or 1 h at RT. Neurofilaments were stained by a rabbit anti-neurofilament medium chain at 1:500 dilution at 4 °C overnight and Alexa 488-labeled goat anti-rabbit F(ab') at 1:400 dilution for 1 h at RT. Primary mouse embryonic cortical neurons were isolated from C57/B6SJL embryos (E14.5) and seeded in 6-well plates at a density of 1.1×10^6 per cm^2 in neurobasal medium plus B27 and 0.5 mM L-glutamine for 36 h. The medium was changed and 10 μM Ara-c was added and cultured for another for another 6 days with medium change every two days. Ara-c was removed and the cells were cultured in neurobasal medium plus B27 in the presence of testing material (ANG or ANG + mAb17) for additional 6 days. For hypothermia-induced degeneration, cells were put at RT for 40 min and returned to 37 °C for additional 4 h. Neurofilaments were stained as described above.

PLXNB cloning and overexpression—Plasmids containing *PLXNB1* (hg01339), *PLXNB2* (hg00246), and *PLXNB3* (hg04331) cDNA were purchased from Kazusa Research Institute (http://www.kazusa.or.jp/e/index.html). The coding regions of the three genes were cloned using the following primers. *PLXNB1*: forward 5' TCTAGAGTCGACatgcctgctctgggcccagctc-3', reverse 5'-TTAAGCGGCCGCctatagatctgtgaccttgttttc-3'; *PLXNB2*: forward 5'-TCTAGAGTCGACatggcactgcagctctgggc-3', reverse 5'-TTAAGCGGCCGCtcagaggtcagtgaccttgttc-3'; *PLXNB3*: forward 5'-TCTAGAGTCGACatgtgccacgccgcccaggag-3', reverse 5'-TTAAGCGGCCGCtcacaggtcagtcactttgttttc-3'. The DNA fragments were inserted into pCI-neo vector (Promega) between the *Sal*I and *Not*I sites. The plasmids were transfected into COS-7 cells using Lipofectamine 2000 (Invitrogen). Stable transfectants were selected with 1.0 mg/ml G418 (Life Technologies). The empty vector pCI-neo was used as the control.

***PLXNB2* knockdown—**The pLKO.1-puro lentiviral vector-shRNA system was used to knockdown *PLXNB2* expression. Two sets of PLXNB2-specific vectors were purchased from Open Biosystems and from Sigma, respectively. The clone numbers of the set from Open Biosystems were TRCN0000048-188, -189, -190, -191, and -192. The clone numbers of the Sigma Mission set were TRCN00003-81195, -00489, -00490, -00549, and -81150). A non-coding shRNA was used as the control. Lentiviral particles were prepared by transient transfection in 293 FT cells using the ViraPower Lentiviral Expression Systems according to manufacturer's instruction (Invitrogen). 293FT cells were cultured in a 10 cm tissue culture plate to 90% confluence without antibiotics, rinsed with fresh medium, put in 5 ml fresh medium, and transfected with a DNA-Lipofectamine 2000 mixture, which was prepared by mixing 3 μg of lentiviral vector-shRNA, 9 μg of the ViraPower Packagin Mix, and 36 μl Lipofectamine 2000 according to according to manufacturer's instruction (Invitrogen). Lentiviral particles were harvested after 72 h, centrifuged at 781 × g for 15 min, and filtered through a 0.45 μm PVDF membrane (Millipore). The viral particles were then ultracentrifuged at 83,000 × g for 1.5 h and the pellet was resuspended in PBS. Stable cell lines were selected with 1.0 μg/ml puromycin (Life Technologies) in regular culture

medium. Three of the 5 clones from Open Biosystems (TRCN0000048-189, -190, and -192), and 3 of the 5 clones from Sigma (TRCN0003-489, -549, and -1500) had satisfactory knockdown efficiency (>90% by RT-PCR and immunoblotting). For most of the experiments clone TRCN00000190 and TRCN000300549 were used. In U87MG cells, PLXNB2 knockdown was also achieved with a doxycycline-inducible pGIPZ vector containing shRNA sequence specific to *PLXNB2* (Addgene). pGIPZ lentiviral particles were packaged in 293T cells with the generation II packaging plasmids (psPAX2 and pMD2.G) and concentrated by Lenti-X concentrator (Clontech). Cells were infected with lentiviral particles for 24 h in the presence of Polybrene (8 μg/ml, Millipore). The medium was replaced with complete growth medium and incubated for 24 h and then selected for 4 days with 1 μg/ml puromycin. GFP-positive cells were visualized under a fluorescence microscope.

Proteins and peptides—Human recombinant ANG and RNASE4 were prepared and purified to homogeneity in house. The purity of ANG and RNASE4 was assessed by silver staining of SDS-PAGE, and confirmed by amino acid analysis to be greater than 99%. The biochemical and biological activity of each ANG preparation was confirmed by ribonuclease assay with yeast tRNA as the substrate and *in vitro* angiogenesis assay. It is notable that a batch of commercially available ANG (R&D Systems) has higher ribonucleolytic activity but 10-fold lower angiogenic activity on chick chorioallantoic membrane (CAM) angiogenesis assay. ANG variants (H13A, R66A and N68D) were generated through site-directed mutagenesis followed by expression and purification as described with WT ANG.

The ECD domains of human recombinant PLXNB2 and PLXNB3 were purchased from R&D Systems. Peptides were chemically synthesized (Peptide 2.0 Inc) with the following sequences. Hplb2-15-02, YTGTREARDIFYKPF; hplb2-15-03, HGDIQCGGHAPGSSK; hplb2-15-04, SFPCGSEHLPYPLGS; hplb2-15-05, RDGLRGTAVLQRGGL; hplb2-15-06, TSSEYDSILVEINKR.

Protein synthesis analysis—Mx1-specific WT or *Plxnb2*$^{-/-}$ LKS or myeloid-restricted progenitor cells were plated as described above in DMEM (Sigma) in the presence or absence of 0.3 μg/ml ANG for 2 hours at 37°C/5% CO^2. After washing cells once with Ca^{2+}- and Mg^{2+}-free PBS, samples were cultured for 1 hour with OP-Puro (50 μM, Medchem Source). After fixing cells in 0.5 ml of 1% paraformaldehyde in PBS for 15 minutes on ice, washing once in PBS, and permeabilizing with 200 μl PBS supplemented with 3% FBS and 0.1% saponin (Sigma) for 5 minutes at RT, cycloaddition of AF488-conjugated azide (5 μM, Life Technologies) was performed using the Click-iT Cell Reaction Buffer Kit (Life Technologies), per manufacturer's instructions. After the cycloaddition, cells were washed twice in PBS/2% FBS/0.1% saponin and subsequently analyzed on a FACSAria flow cytometer. AF488 geometric means were calculated and background fluorescence from cells not cultured with OP-Puro was subtracted from each sample. Values were normalized relative to WT untreated LKS cells. Unpaired two-tailed Student's t-test was used for statistical analysis. *$p<0.05$, **$p<0.01$, ***$p<0.001$.

Quantitative RT-PCR analyses of hematopoietic cells—For qRT-PCR analysis of sorted hematopoietic cell populations, total RNA was extracted using RNeasy Plus Micro

Kit (Qiagen), per manufacturer's instructions. Total RNA was then reverse transcribed into cDNA with Quantitech Reverse Transcription Kit (Qiagen), per manufacturer's instructions. For qRTPCR analysis of rRNA species, random primers (IDT) were used during reverse transcription. For analysis of *Plxnb2* expression in niche cells and central BM, whole BM cells were isolated from femur and tibiae by flushing, and total RNA was extracted by Trizol. For analysis of mixed niche cells, bones were then flushed twice with PBS and were subseqeuntly flushed with 1 ml Trizol. M-MLV reverse transcriptase (Promega) was used to reverse transcribe total RNA into cDNA, per manufacturer's instructions. qRT-PCR analysis was performed on a LightCycler 480 II (Roche) using SYBR Green PCR mix (Roche). Experiments were performed in triplicates with two repeats. Unpaired two-tailed Student's t-test was used for statistical analysis. *$p<0.05$, **$p<0.01$, ***$p<0.001$.

Radioreceptor assays—ANG was iodinated with the use of Iodo-beads (Pierce). The specific activity of ^{125}I-ANG was estimated to be 1.1 μCi/μg (0.87 iodine per protein molecule). LNCaP cells were seeded in 96 well plates at a density of 5×10^3 per well in 100 μl, cultured at 37 °C in phenol red-free RPMI1640 + 10% charcoal/dextran stripped FBS for 24 h, washed with pre-chilled medium and incubated at 4 °C for 10 min. ^{125}I-ANG (0.001 – 2.5 μg/ml, 0.071 – 278 nM) was added to the cells and incubated at 4 °C for 30 min. Cells were washed 3 times and solubilized. Radioactivity was determined with a gamma counter, and the amount of total cell-associated ANG was calculated based on the specific activity of ^{125}I-ANG. Non-specific binding of ^{125}I-ANG to the cells at each concentration was determined by including unlabeled ANG at 10-fold concentration of the corresponding ^{125}I-ANG.

In the experiments to examine the binding of ANG to COS-7 cells transfected with PLXNB1, PLXNB2, and PLXNB3, and to PLXNB2 knockdown LNCaP cells, biotinylated ANG was used instead with ^{125}I-ANG. Biotin-ANG was prepared using Biotin (long Arm) NHS (Vectorlabs) according to manufacturer's protocol. The purity of Biotin-ANG was examined by SDS-PAGE. The biochemical and biological activity of each ANG preparation was confirmed by ribonuclease assay with yeast tRNA as the substrate and *in vitro* angiogenesis assay. The amount of Biotin-ANG bound to cell surface was measured by streptavidin-alkaline phosphatase. The binding experiments were performed in triplicates and repeated three times.

Rota-rod test—WT C57BL/6 mice were treated with PBS control or mAb17 at 30 mg/kg, once every three days, i.p., for two weeks. At the end of treatment, body weight of each mouse was recorded. All the mice were than tested for their neuromuscular function on a Rota-rod (Med Associates Inc). The speed of the rota-rod was set at 20 rpm constantly without acceleration. After a trial session, animal were test for the time they were able to stay on the rotating rod. A cut-off time of 2000 seconds were used. After two successive rota-rod test, PB and BM were collected, and mature cell subsets in the PB and BM and primitive cell subsets in the BM were determined by flow cytometry as described below.

Serial deletion mutants of *PLXNB2*—Full length *PLXNB2* cDNA was cloned into pCI-neo vector as described above. Serial deletion mutants were prepared by 2-step PCR method using the following primers. ΔSema (PSI-IPT remained, Mut1): forward 5'-

CCTGCACCCAGTGCCGCGACAGCAGGTGCGTGTATGAGGC-3', reverse 5'-CCCGGCCTCTGTTCTGAGCAGCAGGGGGCCCGTCTCAGGCTG-3'; ΔPSI-IPT (Sema remained, Mut2): forward 5'-CTCTACCAGCTGGATGCGAAGGTGTTCCGGCTGCCGGTGCAG-3', reverse 5'-GAGATGGTCGACCTACGCTTCCACAAGGCCGACGGCCACGTC-3'; ΔSema-PSI (IPT remained, Mut 3): forward : 5'-CAGCCTGAGACGGGCCCCCTGCTGCTCAGAACAGAGGCCGGG-3', reverse 5'-CCCGGCCTCTGTTCTGAGCAGCAGGGGGCCCGTCTCAGGCTG-3'; ΔSemaΔIPT (PSI remained, Mut4): forward 5'-CCTGCACCCAGTGCCGCGACAGCAGGTGCGTGTATGAGGC-3', reverse 5'-GCCTCATACACGCACCTGCTGTCGCGGCACTGGGTGCAGG-3'; Δ34-133: forward 5'-CTTCTTCCGCAGCGAGAAAGAGTACGAGGACGGCAGCGGGGAG-3', reverse 5'-CTCCCCGCTGCCGTCCTCGTACTCTTTCTCGCTGCGGAAGAAG-3'; Δ134-233: forward 5'-CAACATCTCCCTCCGCCTGTTCCAGCAGGACAAGCACCCGGC-3', reverse 5'-GCCGGGTGCTTGTCCTGCTGGAACAGGCGGAGGGAGATGTTG-3'; Δ234-333 forward 5'-CTACGTCTTCTTTGTCTTCAACACCCGGGAGGCCCGTGACATC-3', reverse 5'-GATGTCACGGGCCTCCCGGGTGTTGAAGACAAAGAAGACGTAG-3'; Δ334-449: 5'-GCAACGCCTGTTACACAGGCCTGGGCAGCCTGTACGCCATG-3', reverse 5'-CATGGCGTACAGGCTGCCCAGGCCTGTGTAACAGGCGTTGC-3'. These mutants were transfected into COS-7 cells using lipofectamine and stable transfectants were selected with G418 as described above.

Silver staining of nucleolar organizer region (NOR)—Formalin-fixed tissue sections were de-paraffinized in xylene, rehydrated successively in ethanol and water, immersed in 10 mM sodium citrate buffer, pH 6.0, and autoclaved in at 120°C for 20 min. After extensive wash with water, the slides were incubated at 37°C for 13 min in a solution containing 1 volume of 2% gelatin in 1% aqueous formic acid, and 2 volume of 0.5 g/ml silver nitrate.

Stem and progenitor staining—Cells were stained for 90 minutes on ice with antibodies against cKit BV711 (BD), Sca1 PE-Cy5 (eBioscience), Flk2 PE (BD), CD34 e660 (eBioscience), IL7R APC-Cy7 (eBioscience), B220 BV785 (Biolegend), CD16/32 AF700 (eBioscience) and a biotinylated lineage cocktail (B220, CD3, CD4, CD8, Mac1, and Ter119 at 1:1:1:1:1:1), followed by staining with streptavidin PE-Cy7 (Biolegend) for 15 minutes on ice. Cells were analyzed using a FACSAria flow cytometer (BD).

Surface plasmon resonance—For kinetic analyses of the binding between ANG and PLXNB2, the Sema domain of PLXNB2 was immobilized. HBS-EP+ (10 mM Hepes, 150 mM NaCl, 3 mM EDTA, and 0.05% P20, pH 7.4) was used as the running buffer. Individual flow cell of CM5 sensor chip was activated with freshly mixed 50 mM NHS and 200 mM EDC (10 μL/min). The Sema domain of recombinant human PLXNBs at the concentration of 2 μg/mL in NaAC (pH 4.5) was injected onto the activated flow cell (flow cell 2) at the flow rate of 10 μl/min. The remaining active coupling sites were blocked with a 420 s injection of 1 M ethanolamine at 10 μl/min. Flow cell 1 was mock-immobilized and used as a blank for non-specific binding. Low flow rate over night was maintained for the equilibrium of the immobilized proteins. ANG was diluted to the concentration of 98, 195,

391, 781, and 1563 pM, and injected over flow cells 1 and 2 for 420 seconds at a flow rate of 30 μl/min for association. Buffer flow was maintained for 600 seconds for dissociation at a flow rate of 10 μl/min. To remove the bound ANG from the cells, 10 mM glycine-HCl, pH 1.7, was injected for 25 seconds at flow rate of 10 μl/min. The flow cells were than stabilized for 1200 seconds before the second injection. The KD value was evaluated using Biacore T200 evaluation software 1.0, with a model of 1:1 binding. Binding between ANG and the Sema domains of PLXNB1 and PLXNB3 were examined in the same fashion except that PLXNB2 was replaced by PLXNB1 or PLXNB3.

Kinetic analysis of the binding between PLXNB2 and mAb17 was performed on Biacore T200 in the same fashion as described above for binding between PLXNB2 and ANG except that ANG was replaced by mAb17 at concentration of 3.125, 6.26, 12.5, 25, and 50 nM. Surface plasmon resonance experiments were repeated once.

tiRNA gel electrophoresis—Diethylpyrocarbonate-treated water was used for all procedures and electrophoresis tanks were sterilized, per standard RNA methodology. Total RNA was diluted in TBE-urea sample buffer, heated to 65°C for 5 minutes and cooled briefly. A 15% TBE-Urea gel (Invitrogen) was pre-run at 74 V for 60 minutes, samples were loaded and run using 0.5X TBE running buffer. After running samples to the bottom of the gel, the gel was disassembled and equilibrated for 5 minutes in 0.5X TBE, followed by staining with SYBR Gold solution (Invitrogen), per manufacturer's instructions. UV illumination was used to image gels on a Kodak Electrophoresis Documentation and Analysis System 120. Multiple independent experiments were quantified by Image J software (NIH).

Xenograft tumor studies—In the experiment to test the prophylactic activity of PLXNB2 mAb17, 1.5×10^6 PC3 cells in 100 μl of 50% Matrigel (BD Biosciences) were inoculated s.c. on the left flank of each mouse. Treatment with PBS control of PLXNB2 mAb17 (daily s.c. injection of 60 μg per mouse) started immediately after tumor cell inoculation. In the therapy experiments, 1.5×10^6 PC-3 cells or U87 cells in 100 μl HBSS, were inoculated s.c. in the left flank of each mouse. Tumor intake rate was 100%. Tumor growth was monitored by palpation and the volume of palpable tumors was recorded every 3 days by a microcaliber as ($½ \times \text{length} \times \text{width}^2$). Mice were randomly separated into 2 groups when the tumor volume reached ~200 mm^3 on day 25, and treated with either PBS control, PlexinB2 mAb17 at 10 mg/kg once every 3 days, or neamine at 30 mg/kg daily by i.p. injection.

QUANTIFICATION AND STATISTICAL ANALYSIS

The number of biological and/or technical replicates for each experiment is stated in the figure legends.

No blinding was used in any stage of the study.

For immunoblots, Image J (NIH) was used to quantify band intensity. For qRT-PCR analysis, the $2^{-\Delta\Delta Ct}$ method was used to quantitate relative expression, with GPI or β-actin as an internal control.

All bar graphs represent mean ± SEM and all heatmaps (RStudio) represent mean from 2–4 independent experiments, unless otherwise indicated. Unpaired two-tailed Student's t-test (Excel) was used for comparison of two experimental groups, and long rank tests (Graphpad Prism) were used for analysis of Kaplan-Meier survival curves. No specific inclusion and exclusion criteria were used for any data or subjects. No methods were used assumptions were made to determine whether the data met assumptions of the statistical approach. For all analyses, *p<0.05, **p<0.01, ***p<0.001, and ns = not significant.

DATA AND SOFTWARE AVAILABILITY

Mass spectrometry data was analyzed by Mascot and deposited in Mendeley, the DOI number is http://dx.doi.org/10.17632/d4vm62tdb2.1

Supplementary Material

Refer to Web version on PubMed Central for supplementary material.

Acknowledgments

We thank the late Dr. Bert L. Vallee for support; Drs. James F. Riordan, Robert Shapiro, Daniel J. Strydom, James W. Fett, Karen A. Olson and K. Ravi Acharya for discussions; Drs. Soo-Ik Chang, Sigitas Verselis, Anatole Klyosov, David Mottashed, Fabrice Soncin, Rongsong Li, Daria M. Monti, Zhengping Xu, and Takanori Tsuji for their early investigations on ANG receptors. This research was supported in part by NIH grants R01CA105241, R01NS065237, and R01HL135160 (to GH), the Endowment for Research in Human Biology, Inc, Vertex Pharmaceuticals Inc. (to GH), Pfizer's Center for Therapeutic Innovation (to GH), NIH fellowship F31HL128127 (to KAG), Sackler Dean's Fellow Award (to KAG), Sackler Families Collaborative Cancer Biology Award (to KAG and GFH), NSFC Grant #81272674 (to SL), Natalie V. Zucker Award (to SL). GFH is a consultant and stockholder of Fuyuan Biopharmaceuticals and Karma Pharmaceuticals.

References

Daviaud N, Chen K, Huang Y, Friedel RH, Zou H. Impaired cortical neurogenesis in plexin-B1 and -B2 double deletion mutant. Dev Neurobiol. 2016; 76:882–899. [PubMed: 26579598]

Deng S, Hirschberg A, Worzfeld T, Penachioni JY, Korostylev A, Swiercz JM, Vodrazka P, Mauti O, Stoeckli ET, Tamagnone L, et al. Plexin-B2, but not Plexin-B1, critically modulates neuronal migration and patterning of the developing nervous system in vivo. J Neurosci. 2007; 27:6333–6347. [PubMed: 17554007]

Di Scala M, Hidalgo A. Angiogenin Defines Heterogeneity at the Core of the Hematopoietic Niche. Cell Stem Cell. 2016; 19:284–286. [PubMed: 27588743]

Druker BJ, Sawyers CL, Kantarjian H, Resta DJ, Reese SF, Ford JM, Capdeville R, Talpaz M. Activity of a specific inhibitor of the BCR-ABL tyrosine kinase in the blast crisis of chronic myeloid leukemia and acute lymphoblastic leukemia with the Philadelphia chromosome. N Engl J Med. 2001; 344:1038–1042. [PubMed: 11287973]

Fett JW, Strydom DJ, Lobb RR, Alderman EM, Bethune JL, Riordan JF, Vallee BL. Isolation and characterization of angiogenin, an angiogenic protein from human carcinoma cells. Biochemistry. 1985; 24:5480–5486. [PubMed: 4074709]

Frelin C, Herrington R, Janmohamed S, Barbara M, Tran G, Paige CJ, Benveniste P, Zuniga-Pflucker JC, Souabni A, Busslinger M, et al. GATA-3 regulates the self-renewal of long-term hematopoietic stem cells. Nat Immunol. 2013; 14:1037–1044. [PubMed: 23974957]

Friedel RH, Kerjan G, Rayburn H, Schuller U, Sotelo C, Tessier-Lavigne M, Chedotal A. Plexin-B2 controls the development of cerebellar granule cells. J Neurosci. 2007; 27:3921–3932. [PubMed: 17409257]

Goncalves KA, Silberstein L, Li S, Severe N, Hu MG, Yang H, Scadden DT, Hu GF. Angiogenin Promotes Hematopoietic Regeneration by Dichotomously Regulating Quiescence of Stem and Progenitor Cells. Cell. 2016; 166:894–906. [PubMed: 27518564]

Greenway MJ, Andersen PM, Russ C, Ennis S, Cashman S, Donaghy C, Patterson V, Swingler R, Kieran D, Prehn J, et al. ANG mutations segregate with familial and 'sporadic' amyotrophic lateral sclerosis. Nat Genet. 2006; 38:411–413. [PubMed: 16501576]

Hirukawa S, Olson KA, Tsuji T, Hu GF. Neamine inhibits xenografic human tumor growth and angiogenesis in athymic mice. Clin Cancer Res. 2005; 11:8745–8752. [PubMed: 16361562]

Hooper LV, Stappenbeck TS, Hong CV, Gordon JI. Angiogenins: a new class of microbicidal proteins involved in innate immunity. Nat Immunol. 2003; 4:269–273. [PubMed: 12548285]

Hu GF, Riordan JF, Vallee BL. A putative angiogenin receptor in angiogenin-responsive human endothelial cells. Proc Natl Acad Sci U S A. 1997; 94:2204–2209. [PubMed: 9122172]

Ivanov P, Emara MM, Villen J, Gygi SP, Anderson P. Angiogenin-Induced tRNA Fragments Inhibit Translation Initiation. Mol Cell. 2011; 43:613–623. [PubMed: 21855800]

Janssen BJ, Robinson RA, Perez-Branguli F, Bell CH, Mitchell KJ, Siebold C, Jones EY. Structural basis of semaphorin-plexin signalling. Nature. 2010; 467:1118–1122. [PubMed: 20877282]

Kao RY, Jenkins JL, Olson KA, Key ME, Fett JW, Shapiro R. A small-molecule inhibitor of the ribonucleolytic activity of human angiogenin that possesses antitumor activity. Proc Natl Acad Sci U S A. 2002; 99:10066–10071. [PubMed: 12118120]

Kieran D, Sebastia J, Greenway MJ, King MA, Connaughton D, Concannon CG, Fenner B, Hardiman O, Prehn JH. Control of motoneuron survival by angiogenin. J Neurosci. 2008; 28:14056–14061. [PubMed: 19109488]

Kishimoto K, Liu S, Tsuji T, Olson KA, Hu GF. Endogenous angiogenin in endothelial cells is a general requirement for cell proliferation and angiogenesis. Oncogene. 2005; 24:445–456. [PubMed: 15558023]

Le AP, Huang Y, Pingle SC, Kesari S, Wang H, Yong RL, Zou H, Friedel RH. Plexin-B2 promotes invasive growth of malignant glioma. Oncotarget. 2015; 6:7293–7304. [PubMed: 25762646]

Li S, Hu GF. Emerging role of angiogenin in stress response and cell survival under adverse conditions. J Cell Physiol. 2012; 227:2822–2826. [PubMed: 22021078]

Li S, Hu MG, Sun Y, Yoshioka N, Ibaragi S, Sheng J, Sun G, Kishimoto K, Hu GF. Angiogenin mediates androgen-stimulated prostate cancer growth and enables castration resistance. Mol Cancer Res. 2013; 11:1203–1214. [PubMed: 23851444]

Marx JL. The 23-million-dollar quest pays off. Science. 1985; 230:161. [PubMed: 4035360]

Olson KA, Fett JW, French TC, Key ME, Vallee BL. Angiogenin antagonists prevent tumor growth in vivo. Proc Natl Acad Sci U S A. 1995; 92:442–446. [PubMed: 7831307]

Perrot V, Vazquez-Prado J, Gutkind JS. Plexin B regulates Rho through the guanine nucleotide exchange factors leukemia-associated Rho GEF (LARG) and PDZ-RhoGEF. J Biol Chem. 2002; 277:43115–43120. [PubMed: 12183458]

Saha B, Ypsilanti AR, Boutin C, Cremer H, Chedotal A. Plexin-B2 regulates the proliferation and migration of neuroblasts in the postnatal and adult subventricular zone. J Neurosci. 2012; 32:16892–16905. [PubMed: 23175841]

Shinoura N, Shamraj OI, Hugenholz H, Zhu JG, McBlack P, Warnick R, Tew JJ, Wani MA, Menon AG. Identification and partial sequence of a cDNA that is differentially expressed in human brain tumors. Cancer Lett. 1995; 89:215–221. [PubMed: 7889532]

Signer RA, Magee JA, Salic A, Morrison SJ. Haematopoietic stem cells require a highly regulated protein synthesis rate. Nature. 2014; 509:49–54. [PubMed: 24670665]

Silberstein L, Goncalves KA, Kharchenko PV, Turcotte R, Kfoury Y, Mercier F, Baryawno N, Severe N, Bachand J, Spencer JA, et al. Proximity-Based Differential Single-Cell Analysis of the Niche to Identify Stem/Progenitor Cell Regulators. Cell Stem Cell. 2016; 530:530–543.

Subramanian V, Feng Y. A new role for angiogenin in neurite growth and pathfinding: implications for amyotrophic lateral sclerosis. Hum Mol Genet. 2007; 16:1445–1453. [PubMed: 17468498]

Trere D, Pession A, Derenzini M. The silver-stained proteins of interphasic nucleolar organizer regions as a parameter of cell duplication rate. Exp Cell Res. 1989; 184:131–137. [PubMed: 2477263]

Tsuji T, Sun Y, Kishimoto K, Olson KA, Liu S, Hirukawa S, Hu GF. Angiogenin is translocated to the nucleus of HeLa cells and is involved in ribosomal RNA transcription and cell proliferation. Cancer Res. 2005; 65:1352–1360. [PubMed: 15735021]

van Es MA, Schelhaas HJ, van Vught PW, Ticozzi N, Andersen PM, Groen EJ, Schulte C, Blauw HM, Koppers M, Diekstra FP, et al. Angiogenin variants in Parkinson disease and amyotrophic lateral sclerosis. Ann Neurol. 2011; 70:964–973. [PubMed: 22190368]

Weiner HL, Weiner LH, Swain JL. Tissue distribution and developmental expression of the messenger RNA encoding angiogenin. Science. 1987; 237:280–282. [PubMed: 2440105]

Yoshioka N, Wang L, Kishimoto K, Tsuji T, Hu GF. A therapeutic target for prostate cancer based on angiogenin-stimulated angiogenesis and cancer cell proliferation. Proc Natl Acad Sci USA. 2006; 103:14519–14524. [PubMed: 16971483]

Zielonka M, Xia J, Friedel RH, Offermanns S, Worzfeld T. A systematic expression analysis implicates Plexin-B2 and its ligand Sema4C in the regulation of the vascular and endocrine system. Exp Cell Res. 2010; 316:2477–2486. [PubMed: 20478304]

Highlights

- PLXNB2 is the receptor of ANG in physiological and pathological cell types
- ANG acts through PLXNB2 to either restrict or promote cell proliferation
- PLXNB2 mediates cell type-specific signaling and RNA processing activities of ANG
- Anti-PLXNB2 therapy is relevant in cancer, neurodegeneration, and stem cells

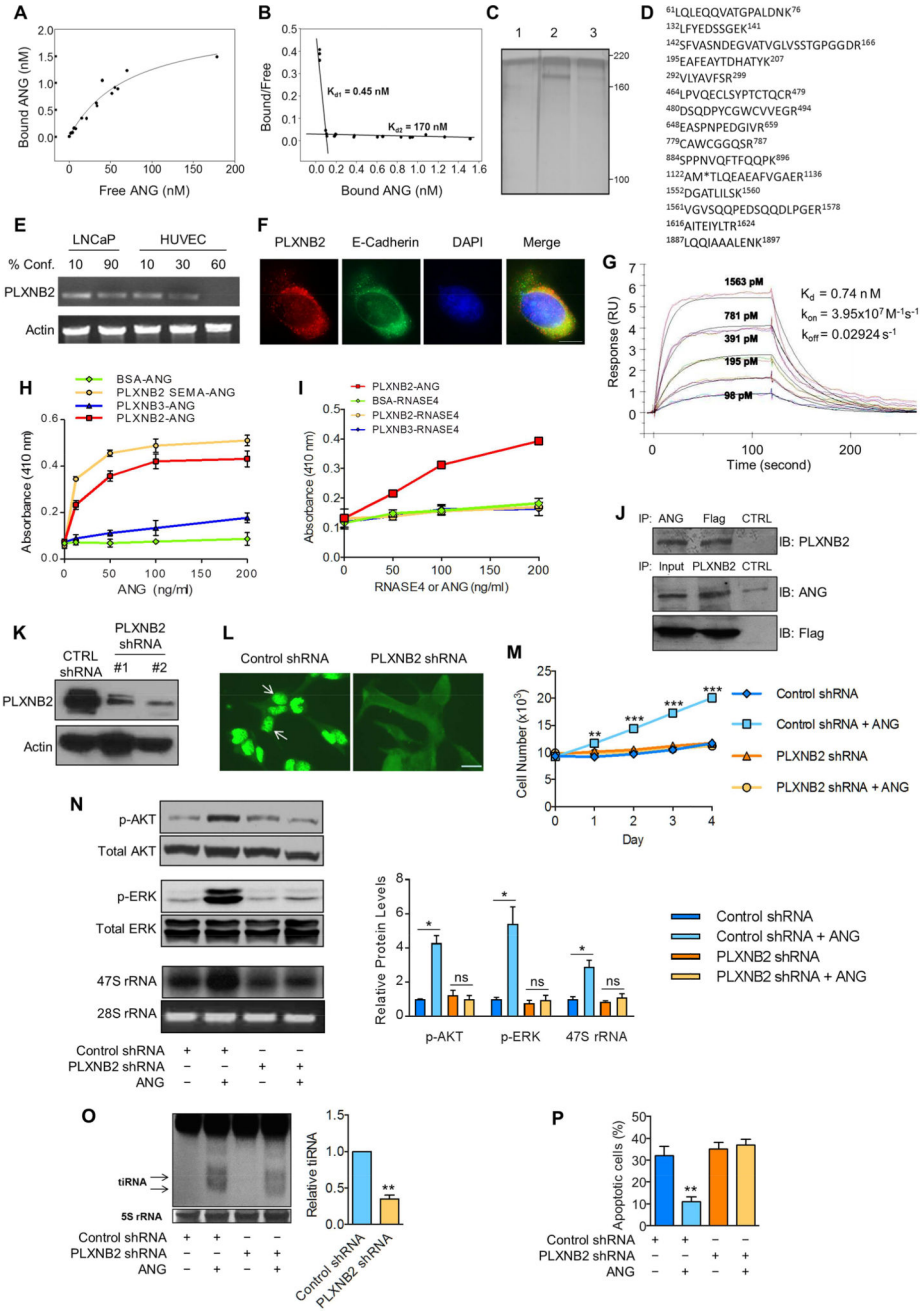

Figure 1. PLXNB2 binds to ANG and mediates its biological activities

(A) Binding of ^{125}I-ANG to LNCaP cell surface.

(B) Scatchard plot of the binding data.

(C) Affinity chromatography of LNCaP cell plasma membrane fraction on ANG-Sepharose (lane 2). Inactivated Sepharose was used as a control (lane 1). Incubation with soluble ANG (0.1 mg/ml) was used to show specificity (lane 3).

(D) Mass spec analysis of the affinity-purified band revealed a total of 15 peptides (from 2 experiments) matching to PLXNB2.

(E) RT-PCR analysis of *PLXNB2* mRNA in LNCaP cells and HUVEC cultured under different cell densities.
(F) IF detection of PLXNB2 on LNCaP cell surface. Arrows indicate PLXNB2 staining. Scale bar = 10 μm.
(G) SPR analysis of binding of ANG to the Sema domain of PLXNB2 analyzed on Biacore T200.
(H) ELISA analyses of ANG binding to ECD and Sema domain of PLXNB2, and to PLXNB3 ECD (n=3).
(I) ELISA analyses of the binding of RNASE4 to PLXNB2 and PLXNB3 (n=3).
(J) Co-IP of ANG-Flag and PLXNB2.
(K) Immunoblot of PLXNB2 in control and two *PLXNB2* knockdown LNCaP cell lines.
(L) Decreased nuclear translocation of ANG in *PLXNB2* knockdown LNCaP cells. Nuclear ANG is indicated by arrows. Scale bar = 20 μm.
(M) Knockdown of *PLXNB2* in LNCaP cells abolished ANG-induced proliferation. Cells were cultured in phenol red-free, charcoal/dextran-treated FBS in the absence of presence of 1 μg/ml ANG. N=5.
(N) Knockdown of *PLXNB2* in LNCaP cells inhibited ANG-induced AKT and ERK phosphorylation, and 47S rRNA transcription.
(O) Knockdown of *PLXNB2* inhibited ANG-mediated tiRNA production (n=5).
(P) Knockdown of *PLXNB2* abolished the protective activity of ANG against serum starvationinduced apoptosis (n=5).
See also Figure S1, S2, and S3.

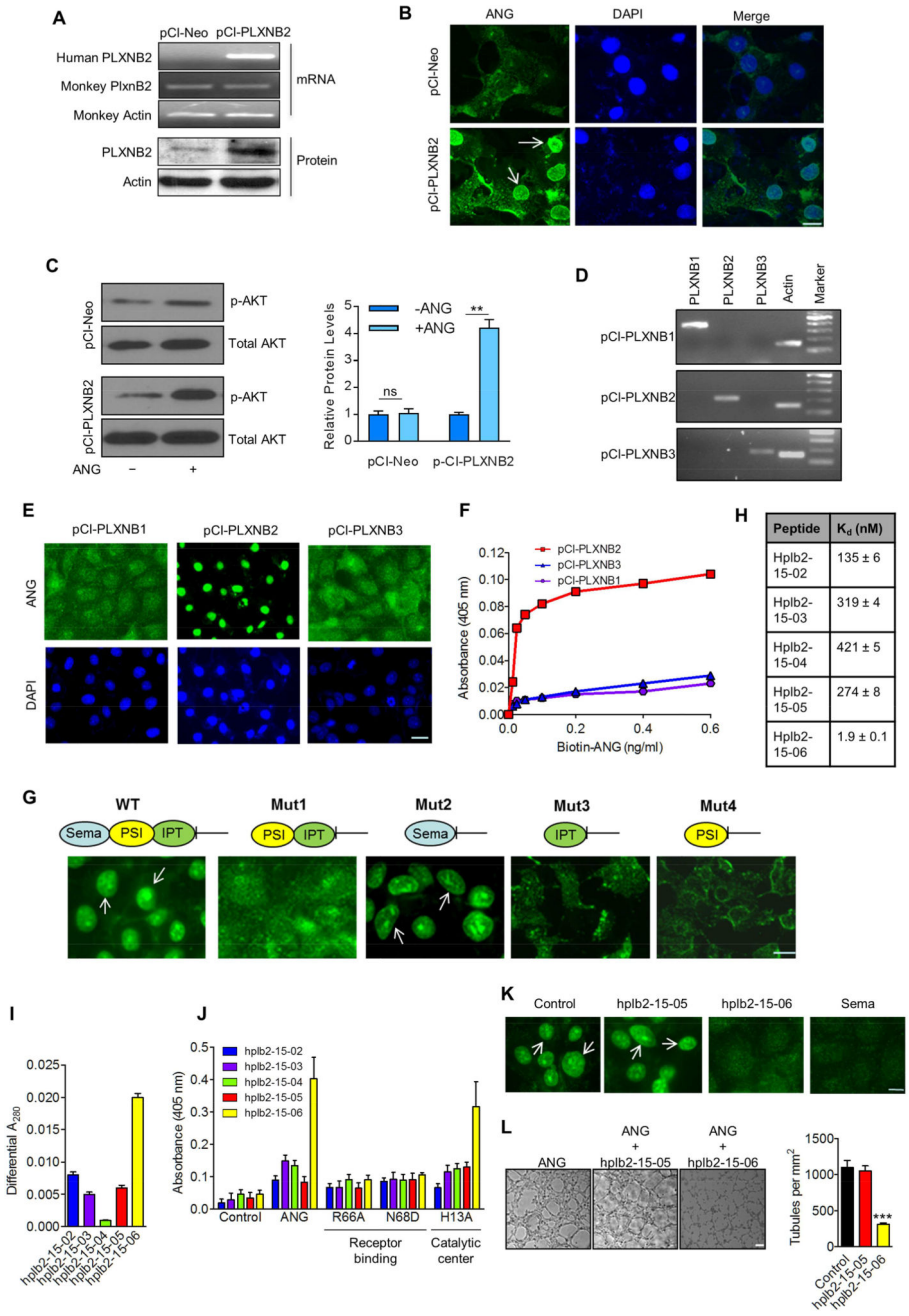

Figure 2. Characterization of PLXNB2 as a functional ANG receptor

(A) Detection of *PLXNB2* mRNA and protein in COS-7 cells transfected with control vector (pCI-Neo) or human *PLXNB2* cDNA (pCI-PLXNB2).

(B) *PLXNB2* transfection enabled nuclear translocation of ANG in COS-7 cells. Nuclear ANG is indicated by arrows. Scale bar = 20 μm.

(C) ANG induced AKT phosphorylation in *PLXNB2* but not vector transfectants of COS-7 cells.

(D) RT-PCR analyses of human *PLXNB1*, *PLXNB2*, and *PLXNB3* mRNA in their respective transfectants of COS-7 cells.

(E) ANG is translocated in COS-7 cells transfected with *PLXNB2*, but not in those transfected with *PLXNB2* or *PLXNB3*. Scale bar = 40 μm.
(F) Binding of biotinylated ANG to cell surface of *PLXNB1*, *PLXNB2*, and *PLXNB3* transfectants of COS-7 cells (n=5).
(G) Nuclear translocation of ANG in COS-7 cells transfected with various deletion mutants of *PLXNB2*. Mut1, Sema domain was deleted; Mut2, PSI and IPT domains were deleted; Mut3, Sema and PSI domains were deleted; Mut4, Sema and IPT domains were deleted. Nuclear ANG is indicated by arrows. Scale bar = 20 μm.
(H) Dissociation constants of ANG and PLXNB2 peptides determined by equilibrium dialysis.
(I) Effects of PLXNB2 peptides on UV absorption of ANG determined by differential spectrum (n=3).
(J) ELISA analyses of binding between PLXNB2 peptides and ANG variants R66A, N68D, and H13A (n=3).
(K) ANG-binding peptide hplb2-15-06 and Sema domain of PLXNB2 inhibited nuclear translocation of ANG in HUVEC. Nuclear ANG is indicated by arrows. Scale bar = 20 μm.
(L) ANG-binding peptide of PLXNB2 inhibited ANG-induced HUVEC tubule formation. Scale bar = 100 μm. Tubular structures were counted and presented as bar graphs. Data shown are mean ± SD (n=3).
See also Figure S4.

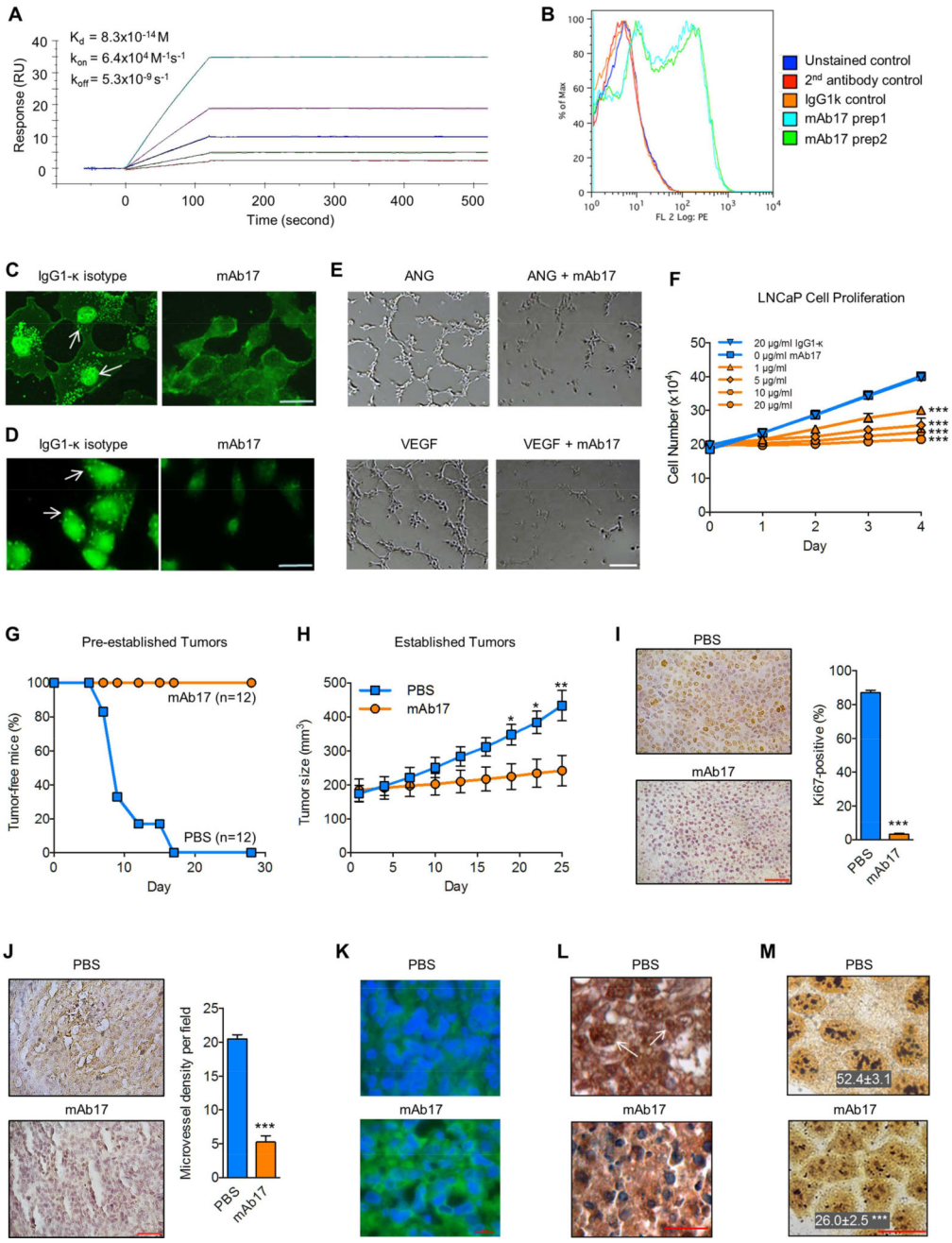

Figure 3. Monoclonal antibodies of the ANG-binding site of PLXNB2 inhibited biological activities of ANG and tumor growth

(A) Binding of mAb17 on PLXNB2 analyzed by SPR.

(B) Binding of mAb17 on LNCaP cell surface analyzed by flow cytometry.

(C) mAb17 inhibited nuclear translocation of ANG in LNCaP cells under growth conditions. Nuclear ANG is indicated by arrows. Scale bar = 20 μm.

(D) mAb17 inhibited SG localization of ANG in LNCaP cells under stress. SG ANG is indicated by arrows. Scale bar = 20 μm.

(E) mAb17 inhibited HUVEC tubule formation induced by ANG and VEGF. Scale bar = 100 μm.

(F) mAb17 inhibited LNCaP proliferation dose-dependently.
(G) mAb17 prevented establishment of PC-3 xenografts in athymic mice (n=12).
(H) mAb17 inhibited growth of established PC-3 xenograft tumors in athymic mice. Treatment was started when tumors reached a size of 200 mm^3 (n=6–12).
(I-J) mAb17 inhibited *in vivo* tumor cell proliferation (I, n=6) and angiogenesis (J, n=6). Scale bar = 200 μm.
(K) Systemically delivered mAb17 targeted to tumor tissues. Tumor tissues from PBS and mAb17-treated mice were stained by mouse IgG. Scale bar = 10 μm.
(L) mAb17 treatment blocked nuclear translocation of ANG in tumor cells *in vivo*. Nuclear ANG is indicated by arrows. Scale bar = 50 μm.
(M) *In vivo* treatment of mAb17 suppressed rRNA transcription in tumor tissues as shown by decreased number of nucleolar organizer region (NOR). Scale bar = 10 μm. Numbers shown are means ± SD of NOR dots per nucleus (n=20).
See also Figure S5 and S6.

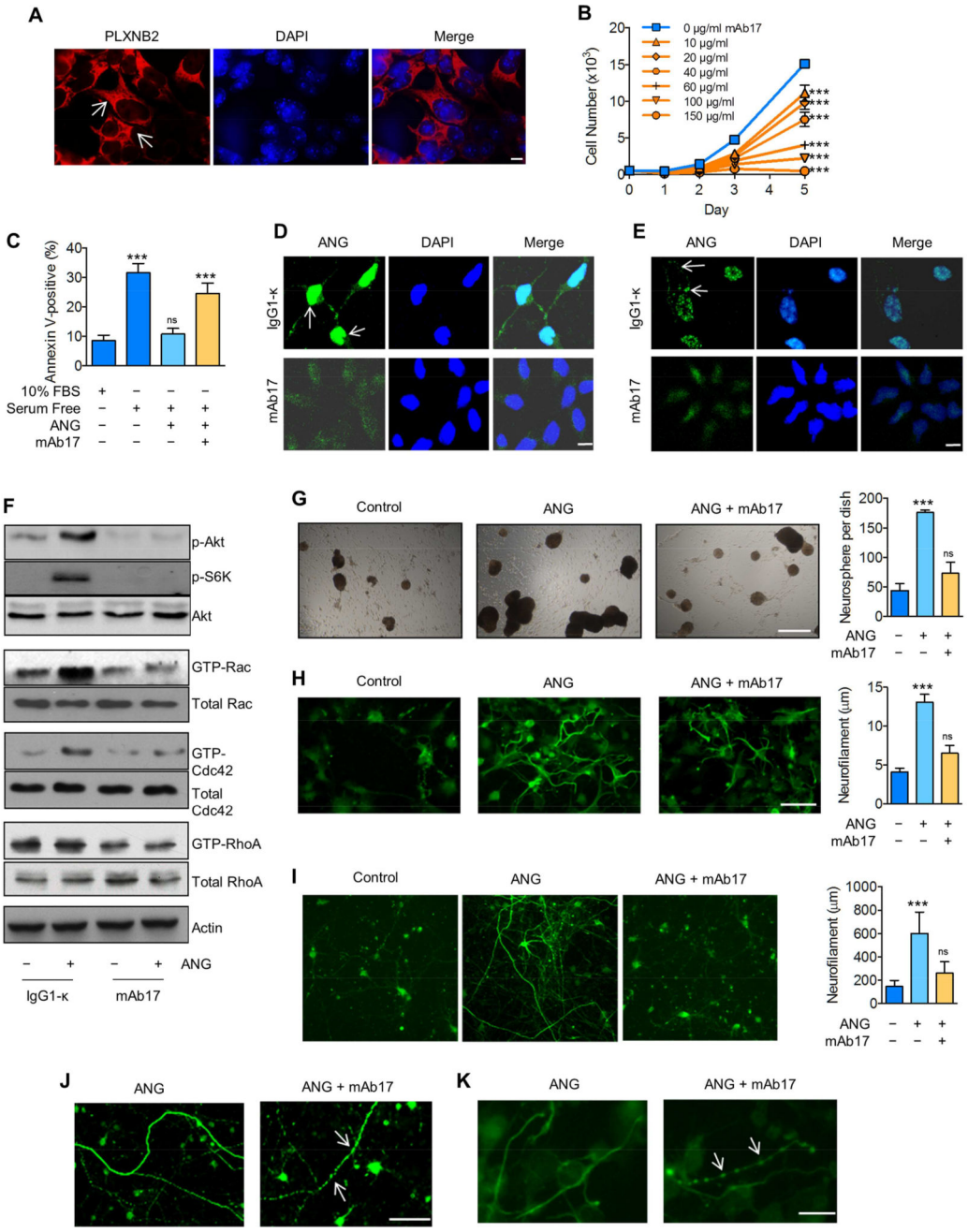

Figure 4. PLXNB2 mAb17 inhibits neurological activities of ANG

(A) IF detection of mouse PLXNB2 in P19 cells by mAb17. Scale bar = 10 μm.

(B) Dose-dependent inhibition of P19 cell proliferation by mAb17 (n=5).

(C) Effect of mAb17 on protective activity of ANG against serum starvation-induced apoptosis. Data shown are mean ± SD of percentages of Annexin V positive cells (n=5).

(D) mAb17 inhibited nuclear translocation of ANG in P19 cells under growth conditions. Nuclear ANG is indicated by arrows. Scale bar = 10 μm.

(E) mAb17 inhibited SG localization of ANG in P19 cells under stress. SG ANG is indicated by arrows. Scale bar = 10 μm.

(F) mAb17 inhibited ANG-stimulated AKT, S6K, Rac, and Cdc42 activation in P19 cells.
(G) mAb17 inhibited ANG-stimulated neurosphere formation of P19 cells. Scale bar = 250 μm (n=3).
(H-I) mAb17 inhibited ANG-stimulated neurite outgrowth in P19 cells (H) and neurofilament extension of mouse embryonic cortical neurons (I). Scale bars = 10 μm (H) and 250 μm (I) (n=20).
(J-K) mAb17 abolished the protective activity of ANG against stress-induced neurofilament fragmentation of mouse embryonic cortical neurons (J) and P19-derived neurons (K). Neurofilaments were induced by B27 and subjected to hypothermic stress (16 °C) in the presence of ANG or ANG plus mAb17. Arrows mark fragmentation of neurofilaments. Scale bars = 200 μm (J) and 10 μm (K) (n=20).

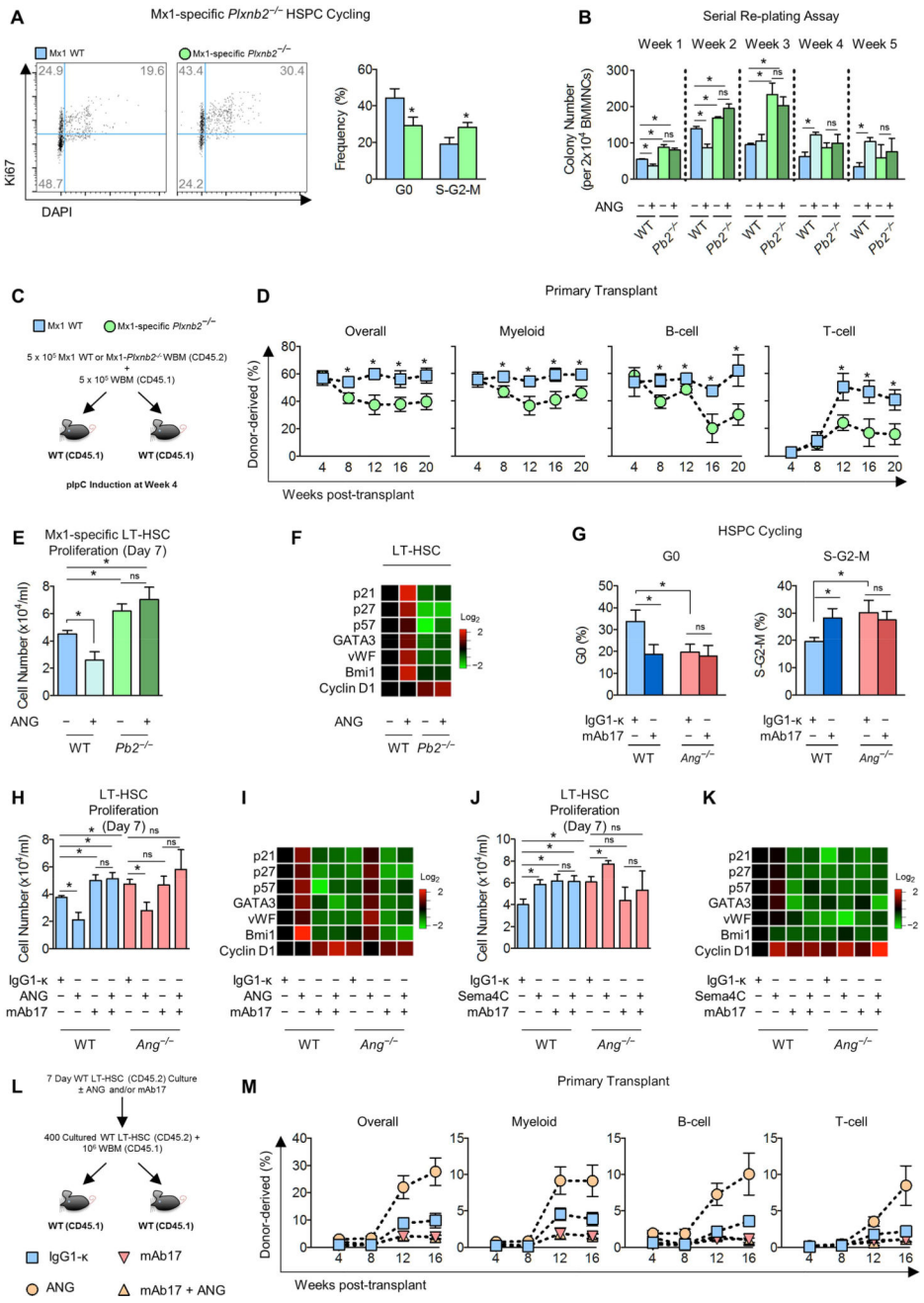

Figure 5. ANG regulates primitive hematopoietic cell properties through PLXNB2

(A) Quantification of HSPC cell cycle status of Mx1-specific *Plxnb2*$^{-/-}$ mice (n=9).

(B) Serial re-plating colony assay of whole BM cells (n=2). ANG was added at each re-plating.

(C) Experimental schema of transplant using Mx1-specific *Plxnb2*$^{-/-}$ whole BM as donors.

(D) Multi-lineage donor cell chimerism after competitive transplant of Mx1-specific *Plxnb2*$^{-/-}$ donors (n=5).

(E-F) ANG (0.3 μg/ml) regulates LT-HSC proliferation (E, n=3) and pro-self-renewal transcripts (F, n=3) from WT but not from Mx1-specific *Plxnb2*$^{-/-}$ mice.

(G) Quantification of HSPC cell cycle status of mAb17-treated WT or *Ang*$^{-/-}$ mice (n=6).
(H-I) Cell density on day 7 (H, n=3) and qRT-PCR analysis of pro-self-renewal transcripts (I, n=3) from sorted WT or *Ang*$^{-/-}$ LT-HSC cultured in the presence of 0.3 μg/ml ANG, 50 μg/ml mAb17, or both.
(J-K) Cell density on day 7 (J, n=3) or qRT-PCR analysis of pro-self-renewal transcripts (K, n=3) from sorted WT or *Ang*$^{-/-}$ LT-HSC cultured in the presence of 0.3 μg/ml Sema4C, 50 μg/ml mAb17, or both.
(L) Experimental schema of transplant using sorted WT LT-HSC that had been cultured with 0.3 μg/ml ANG, 50 μg/ml mAb17, or both for 7 days.
(M) Multi-lineage donor cell chimerism after competitive transplant of ANG and/or mAb17-treated WT LT-HSC donors (n=6).
See also Figure S7.

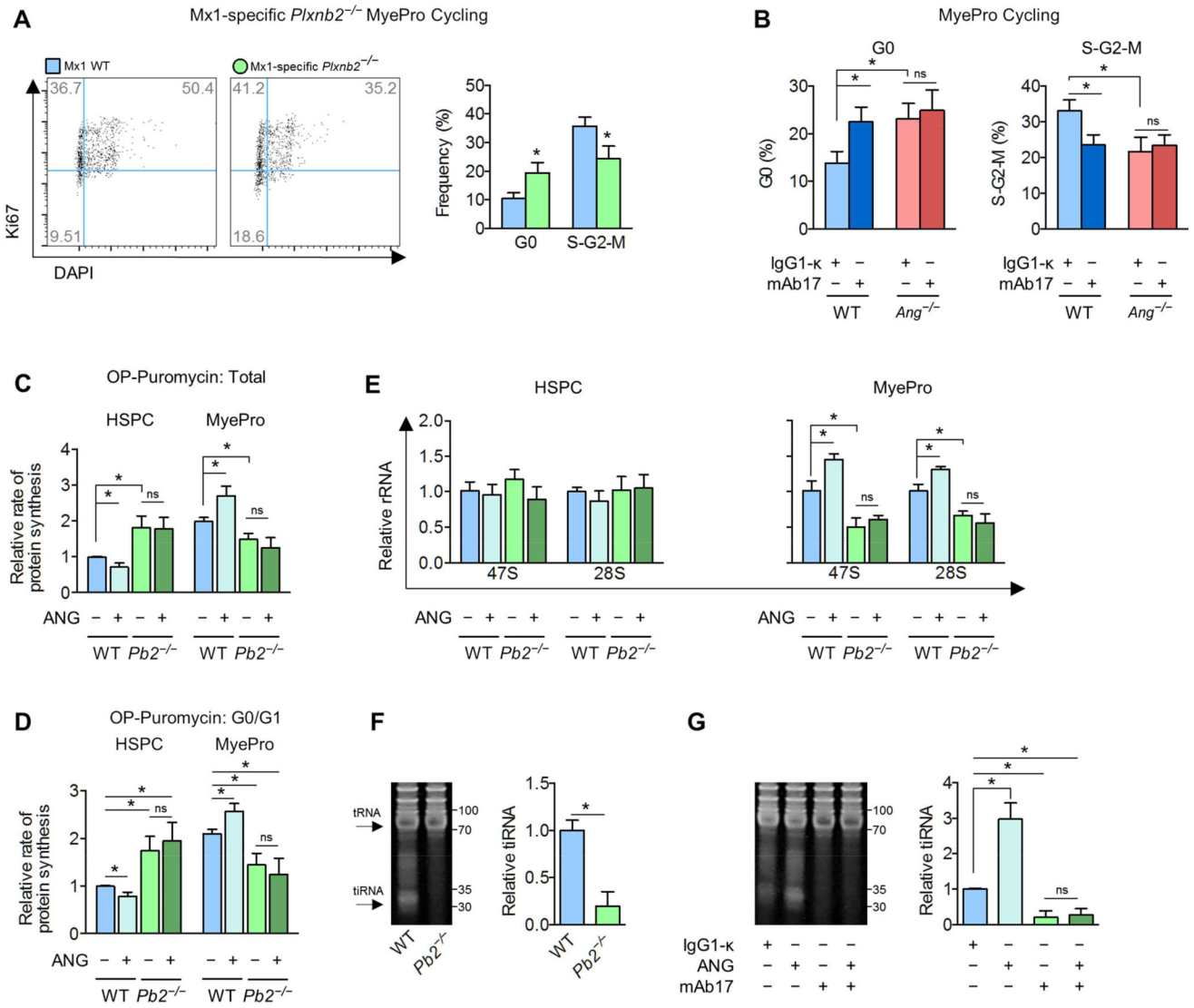

Figure 6. Cell type-specific regulation of protein synthesis by ANG-PLXNB2

(A-B) Quantification of MyePro cell cycle status of WT and Mx1-specific *Plxnb2*$^{-/-}$ (A, n=9) and mAb17-treated WT or *Ang*$^{-/-}$ mice (B, n=6).

(C-D) OP-Puro incorporation following 2 h ANG treatment of WT or Mx1-specific *Plxnb2*$^{-/-}$ HSPC and MyePro for cells in all phases (C, n=4) or in G0/G1 phase (D, n=4).

(E) qRT-PCR analysis of rRNA following 2 h ANG treatment of WT or Mx1-specific *Plxnb2*$^{-/-}$ HSPC and MyePro (n=3).

(F-G) Small RNA production in Mx1-specific *Plxnb2*$^{-/-}$ HSPC (F, n=2) or WT HSPC treated with 0.3 μg/ml ANG, 50 μg/ml mAb17, or both (G, n=2).

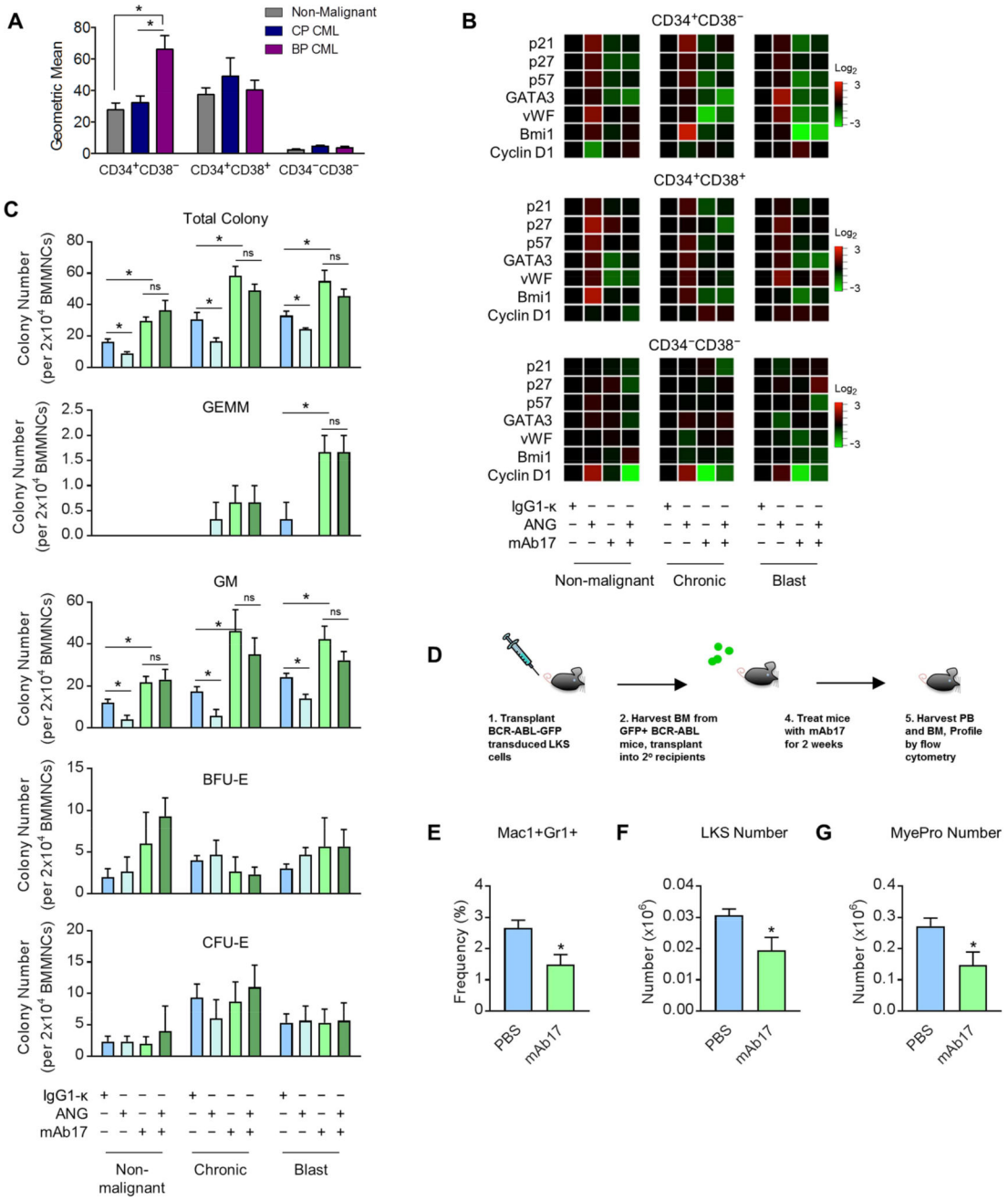

Figure 7. ANG-PLXNB2 regulates leukemic stem cell properties

(A) PLXNB2 expression in leukemic stem/progenitor cells from BM aspirates of non-malignant controls and patients diagnosed with chronic and blast phase CML (n=3–4).

(B) qRT-PCR analysis of pro-self-renewal transcripts from sorted leukemic stem/progenitors ($CD34^+CD38^-$ and $CD34^+CD38^+$), and differentiated cells ($CD34^-CD38^-$) cultured in the presence of 0.3 μg/ml ANG, 50 μg/ml mAb17, or both for 2 days (n=3).

(C) Colony formation of bone marrow cells from CML patients and non-malignant control subjects cultured in the presence of 0.3 μg/ml ANG, 50 μg/ml mAb17, or both (n=3).

(D) Experimental schema of BCR-ABL mouse model.

(E-G) Quantification of GFP^+ myeloid cell frequency in PB (E), and GFP^+ LKS (F) or GFP^+ MyePro (G) number in BM of mAb17-treated mice (n=5–6).